Distribution Agreement

In presenting this thesis as a partial fulfillment of the requirements for a degree from Emory University, I hereby grant to Emory University and its agents the non-exclusive license to archive, make accessible, and display my thesis in whole or in part in all forms of media, now or hereafter now, including display on the World Wide Web. I understand that I may select some access restrictions as part of the online submission of this thesis. I retain all ownership rights to the copyright of the thesis. I also retain the right to use in future works (such as articles or books) all or part of this thesis.

Joseph G. Piccolo December 3, 2020

Electromagnetic Tweezer Development: Improving Single-Molecule Techniques for the Study of DNA Mechanics and Gene Transcription

by

Joseph G. Piccolo

Laura Finzi
Adviser

Department of Physics

Laura Finzi
Committee Member

David Dunlap
Committee Member

Effrosyni Seitaridou
Committee Member

Sean Mo
Committee Member

Dana Haugaard
Committee Member

2020

Electromagnetic Tweezer Development: Improving Single-Molecule Techniques for the Study of DNA Mechanics and Gene Transcription

By

Joseph G. Piccolo

Laura Finzi
Adviser

An abstract of
a thesis submitted to the Faculty of Emory College of Arts and Sciences
of Emory University in partial fulfillment
of the requirements of the degree of
Bachelor of Science with Honors

Department of Physics

2020

Abstract

Electromagnetic Tweezer Development: Improving Single-Molecule Techniques for the Study of DNA Mechanics and Gene Transcription

By Joseph G. Piccolo

DNA transcription is the foundational biological process to all cellular life. Transcription and eventual gene expression are regulated via proteins known as transcription factors. DNA torsion and tension play an important role in the binding and unbinding of transcription factors. The interplay between these physical parameters and transcription factors is key to the understanding of transcriptional regulation; yet, it is extremely hard to study in vivo. Bulk in vitro measurements are the averages of an Avogadro's number scale of molecules, a scope that obscures individual molecular details. Thus, single-molecule techniques have emerged as powerful approaches to study molecular mechanisms. A magnetic tweezer is a single molecule technique which allows application of tension and torque to individual DNA molecules in solution. The most common setup, a pair of permanent rare-earth magnets, is positioned near the sample, above an optical microscope stage using motorized mechanical translators. Unfortunately, the electric motor introduces unwanted vibrations into the system, reducing the accuracy of measurements. This thesis describes the development of an electromagnetic tweezer that eliminates physical motion within the optical system and includes custom electromagnetic solenoids, control electronics, as well as ad hoc software. The ability of these electromagnetic tweezers to stretch and twist DNA was tested in preliminary measurements and possible applications of this instrument in the study of transcription and its regulation are discussed.

Electromagnetic Tweezer Development: Improving Single-Molecule Techniques for the Study of DNA Mechanics and Gene Transcription

By

Joseph G. Piccolo

Laura Finzi
Adviser

A thesis submitted to the Faculty of Emory College of Arts and Sciences
of Emory University in partial fulfillment
of the requirements of the degree of
Bachelor of Science with Honors

Department of Physics

2020

Acknowledgements

My thanks to Laura Finzi, David Dunlap, Josh Mendez, and Daniel Kovari for granting me the opportunity to work with my hands in the study of life. I would also like to thank Effrosyni Seitaridou and Sean Mo for inspiring me to pursue science beyond the lecture halls. To Dana Haugaard, thank you for providing a creative space for me to follow my interests independent of the sciences.

I would also like to extend a thank you to the team of doctors, physical therapists, and occupational therapists that guided me through my healing process.

To my father, Alessandro Piccolo, I give my greatest thanks for his unyielding support through the years.

This research was supported by the National Institute of General Medicine (NIGMS) grant #R01GM084070 to Dr. Laura Finzi and special funding provided by the Emory College of Arts and Sciences Undergraduate Research Program.

Table of Contents

Table of Figures

I. Introduction

A. DNA and The Central Dogma

Life is the consequence of innumerable microscopic interactions. Camouflaged by scale, these tiny interactions combine to form net effects on living organisms spanning from bacteria to blue whales in the sea. One such group of interactions, relevant to *all* life, is those associated with deoxyribonucleic acid, or DNA for short.

DNA is a polymer consisting of individual units known as deoxynucleotides. Each monomer is made up of a phosphate group, a deoxy pentose sugar, and a nitrogenous base. The 'variable' portion of each monomer is the nitrogenous base, which can be adenine (A), guanine (G), cytosine (C), or thymine (T). A single-stranded molecule of DNA (ssDNA) is built when the phosphate attached to the 5' carbon forms a phosphodiester linkage with the 3' hydroxyl group of another deoxynucleotide. A and G can hydrogen bond to T and C, respectively, to form a base pair. If the sequence of one ssDNA is complementary to the sequence of another ssDNA, these two single-strands can 'hybridize' in an antiparallel fashion to form double-stranded DNA (dsDNA). A deoxynucleotide and the bonding scheme of DNA are shown in Figure 1. Double-stranded DNA in solution typically adopts a right-handed, double helical conformation known as B-form which has a pitch of approximately 10.4 base pairs (bp) per turn. The sequence of nitrogenous bases in the genome forms the blueprint of an organism by encoding all the proteins necessary for life.

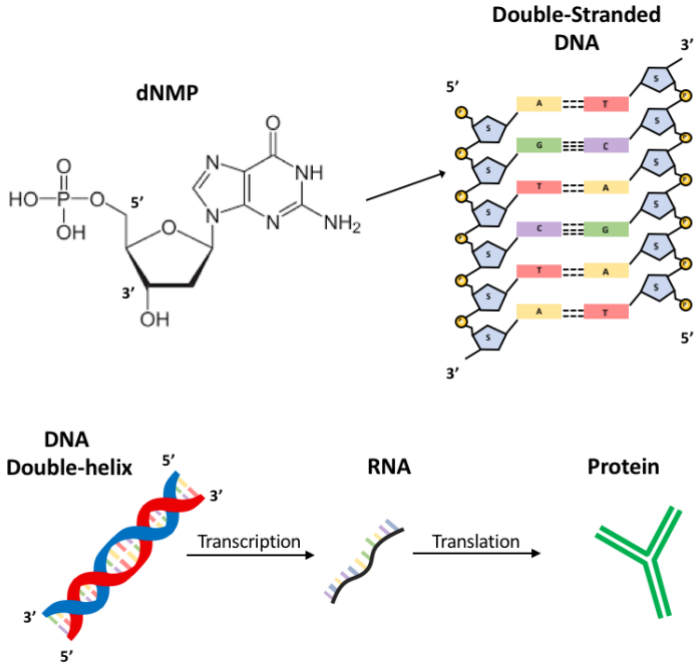

Figure 1: DNA Structure and the Central Dogma - **Top left-** A monomer of DNA, deoxyguanosine monophosphate, is shown with the 5' phosphate and 3' hydroxyl labelled. **Top right-**This deoxynucleotide monophosphate (dNMP) along with its antiparallel complement form a rung in the dsDNA ladder. **Bottom-** The information stored in the DNA sequence is transcribed to RNA then translated into protein. This sequence of events is known as the central dogma. The expression of proteins encoded in the genome is highly regulated.

As a tenet of biology, gene expression in nearly all biological systems involves the transcription of DNA into RNA by RNA polymerase (RNAP in prokaryotes), followed by the translation of RNA into proteins. These enzymatic processes constitute the central dogma of biology.[1]

B. DNA Supercoiling

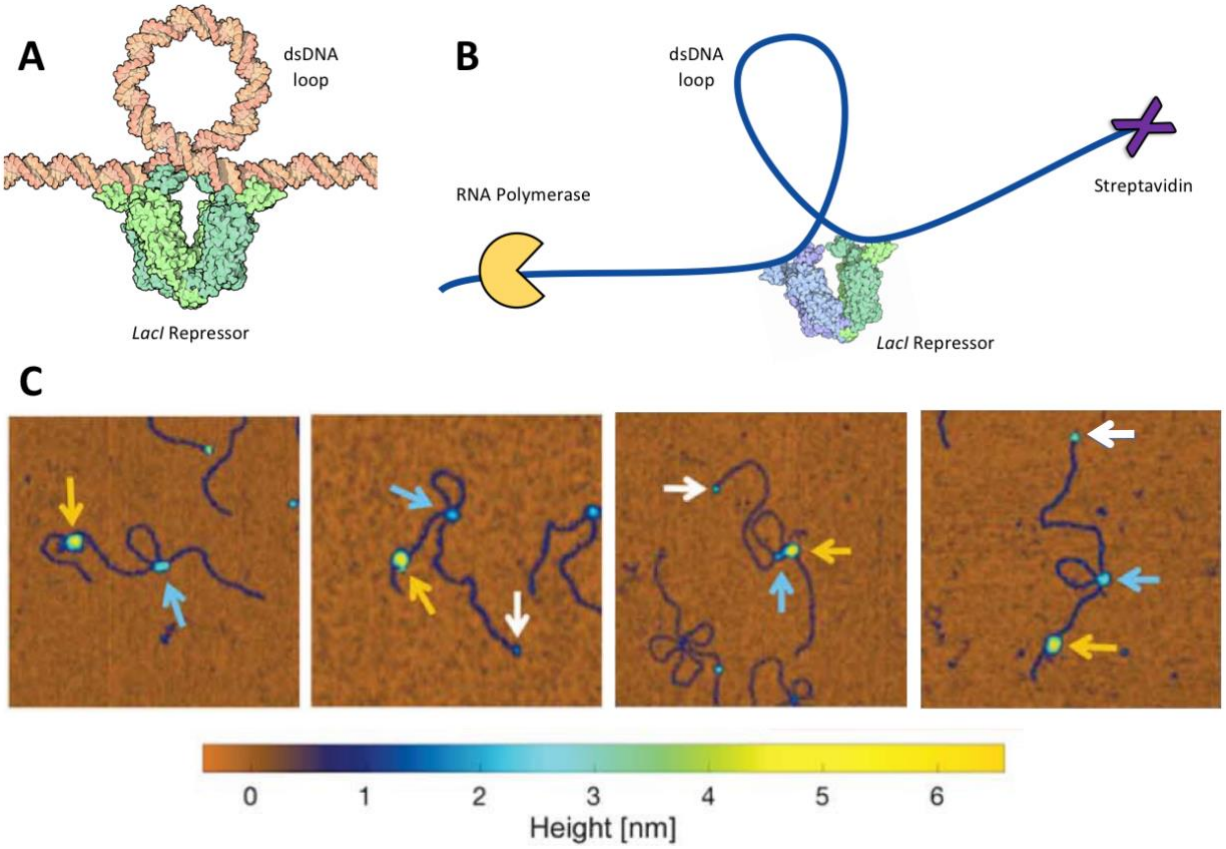

Figure 2: Visualization of DNA Looping - **A**- A 3D model of LacI bound to dsDNA to form a loop. **B**- Diagram of the nucleoprotein complexes imaged by atomic force microscopy images (AFM). dsDNA with a promoter-bound RNAP, LacI-mediated loop, and biotin-streptavidin labelled end. **C**- AFM images of transcription elongation complexes. Yellow arrows indicate RNA polymerase, cyan arrows indicate LacI securing a loop, and white arrows indicate streptavidin. These images were taken by placing the DNA construct on a flat mica surface. The pseudo color scale indicates the relative height of each feature in the image. Portions of this figure were originally published in the following sources and reused here under the terms of the Creative Commons Attribution 4.0 license. "Figure 2: Nanographs of RNAP elongation along DNA with and without LacI-mediated loops" by Vörös et al. 2017 and "Lac repressor" by Goodsell 2003.

DNA topology is dynamically modified by proteins. In particular, several proteins change the twist of DNA, by either winding or unwinding the double helix. These topological modifications affect gene expression and are fundamental mechanisms of gene regulation. Proteins known as transcription factors (TFs) can influence RNAP directly or indirectly through mechanisms that include supercoiling.[2,3] Some TFs bind to DNA and act as road-blocks, and in some cases alter the tension and topology of the

strand creating bends, wraps, or loops.[4–6] The LacI protein in *Escherichia coli* is a classic example of a loop-inducing transcription factor as shown in Figure 2.[4,7]

To understand what role the bending and torsional elasticity of DNA play in protein-induced DNA conformational and topological changes, two theoretical models are particularly useful: the worm-like chain (WLC) model and White's theorem. The WLC model has been employed to accurately describe the behavior of DNA in response to physical manipulations.[8] According to this model DNA is treated as a homogenous, isotropic polymer with a specified bending stiffness.[9] The mathematician James White proved that in a torsionally constrained string in three-dimensions, the linking number is invariant to transformations that do not break the string.[10] It expresses the linking number (*Lk*) as

$$Lk = Tw + Wr\,, \tag{1}$$

in which twist (Tw) is the number of full helical turns of the molecule while writhe (Wr) is the number of times the helical axis crosses over itself. White's theorem is well suited to describe the supercoiling of a dsDNA molecule. In a torsionally relaxed molecule of dsDNA, the linking number is a constant Lk_o, with no writhe (Wr_o = 0) and twist (Tw_o) given by

$$Tw_o = L_{bp}/p_{o,bp} \tag{2}$$

in which the length of the DNA molecule in base pairs (L_{bp}) is divided by the average pitch of the double helix in base pairs $\left(p_{o,bp} = \ 10.4\,\frac{\text{base pairs}}{\text{helical turn}}\right)$.[11] The relative difference between the linking number of a torsionally relaxed molecule and one that is torsionally stressed is defined by the supercoiling density (σ):

$$\sigma = \frac{Lk - Lk_o}{Lk_o}. \tag{4}$$

Supercoiled DNA has

$$Lk \neq \ Lk_o \ \text{ or } \ \sigma \neq 0. \tag{5}$$

Topological changes that can be described with these models include the formation of toroidal and plectonemic loops. The difference between writhe and twist allows us to characterize supercoiled states in DNA, as shown in Figure 3.

Topological changes occur rapidly within individual molecules of double-stranded DNA in the complex cellular environment, and there are no tools with which to visualize conformational dynamics. Instead, *in vitro*, single-molecule techniques[4] are exquisite tools to probe these regulatory structural changes.

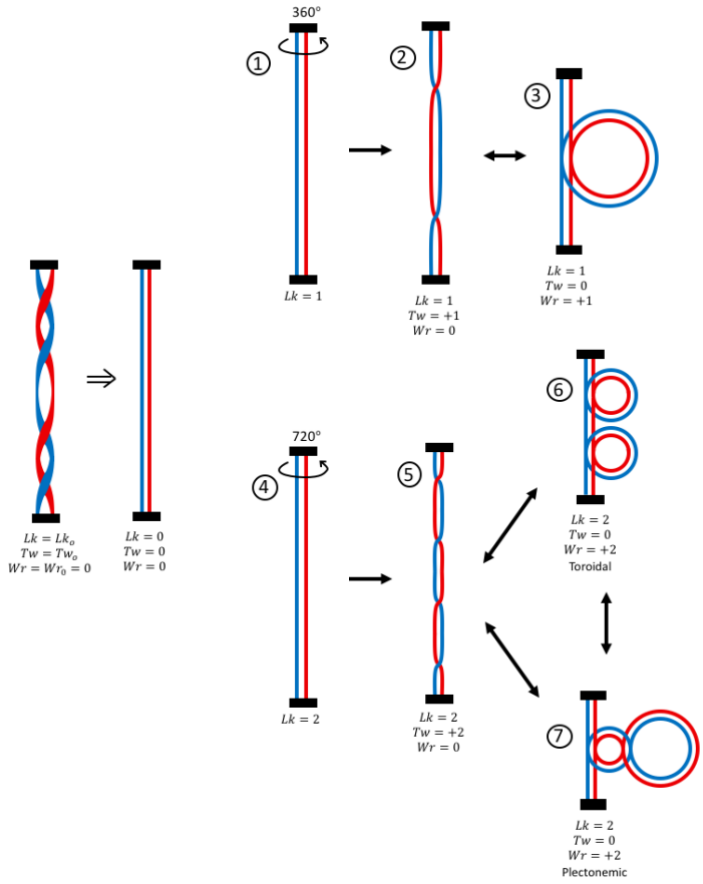

Figure 3: Quantification of DNA Supercoiling - The supercoiling of the right-handed DNA double helix can be quantified using linking number (Lk), twist (Tw), and writhe (Wr). For the visualization of induced supercoiling beyond natural values, the relaxed double helix is simplified to a pair of parallel strings. With one end fixed, a full rotation of the opposing end results in a Lk of 1 (1). By the conservation of Lk by Tw and Wr, 2 conformations of the strings are possible. In an un-looped state (2), the twist increases by 1 manifesting as a double cross. In a looped state (3), the Wr increases by 1, manifesting as a single loop. In a Lk of 2 system (4), Tw and Wr interchange to conserve shape. A quadruple cross represents the fully twisted conformation (5). When Lk exceeds 1, looping may be toroidal (6) or plectonemic (7). All of these transformations influence the overall length between the two ends of DNA.

C. Single Molecule Experimentation/DNA Tethers

A single-molecule technique is an experimental method to measure the behavior/function of a system of interest, one-molecule at a time. In the study of the structure, kinetics, and thermodynamics of nucleoprotein complexes, the single-molecule approach allows for data collection from individual molecules of DNA in the presence of TFs. These single-molecule *in vitro* assays overcome the challenges of interpreting measurements from Avogadro's number scales of unsynchronized molecules. These techniques allow the close investigation of the molecular details of transcriptional regulation. By virtue of their nature, single-molecule approaches allow the discovery of sub-population behaviors that would be otherwise, completely obscured.[12]

One such approach is to characterize nucleoprotein kinetics by monitoring the conformation of a particular DNA segment as it interacts with a relevant protein using DNA tether assays. A DNA tether assay entails attaching a micro-scale bead or tracker particle to one end of a DNA strand while the other is attached to the surface of a microscope flow chamber. This "tether" forms a ball-and-chain type

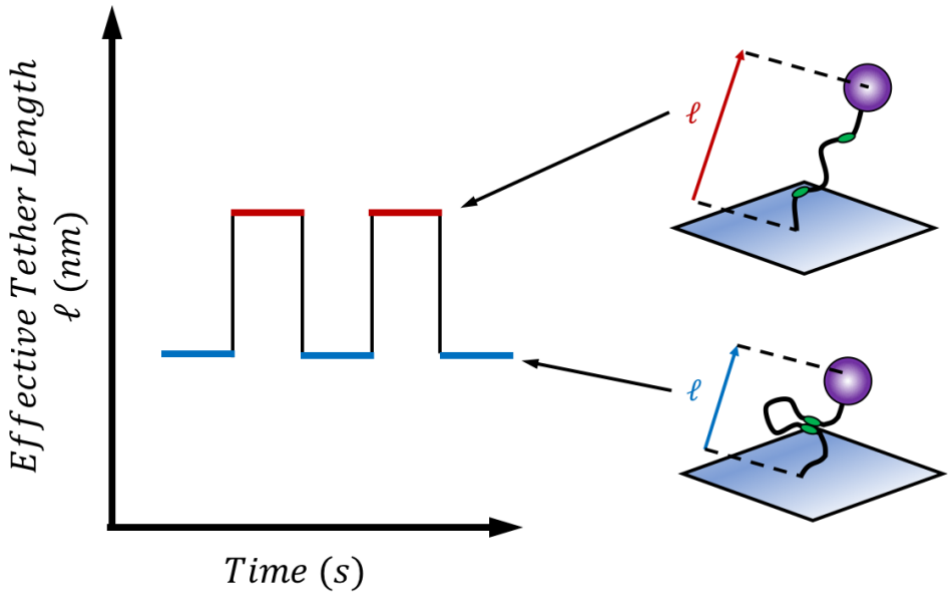

Figure 4: Tethered DNA System - In the study of DNA mechanics, a novel single-molecule system is tethered DNA. A DNA tether consists of a DNA segment specifically bound to a glass surface (blue) and tracker particle (purple) on either end. The tracker particle, visible in various microscopy techniques, executes constrained Brownian motion about the immobilization point. Various motional parameters of the tracker particle are recorded and analyzed to give insight on the DNA's physical attributes. One physical attribute, effective tether length (ℓ), is the length between the immobilization point and tracker particle. When studying a DNA tether, interactions with transcription factors (green) can alter the effective tether length, a quantity measurable in real-time.

system, which can be observed under a microscope. As the bead undergoes thermal Brownian diffusion, its motion is confined by the DNA attachment. The bead's position is monitored as a function of time, providing a measurement of the effective tether length. A hypothetical DNA tether graph is shown in Figure 4 in which the interconversion between two DNA conformational states, such as bent/unbent, wrapped/unwrapped and looped/unlooped by TFs affect the overall effective length of the DNA tether and can be monitored in real time by automated particle tracking. This DNA tether system allows us to dynamically observe DNA conformations with high resolution.

D. Magnetic Tweezers

DNA tether techniques can be extended to interrogate the effect of stretching and twisting by applying tension and torque to the bead. This is most easily done using an optical microscope equipped with magnetic tweezers (MTs). In this case, the bead attached to the freely moving end of the DNA tether is made from a super-paramagnetic material and an arrangement of permanent magnets are mounted above the stage. These magnets generate a magnetic field (B), which interacts with the bead,

effectively allowing the experimenter to handle each microscopic DNA molecule through macroscopic means.

DNA manipulation via MTs can be visualized as a telephone cord immobilized on one end by the telephone body while the other is attached to the handset. One method to change the supercoiling of the telephone cord would be pulling upwards from the body, extending and unwinding the cord through tension. Another method would be by twisting the handset in the same (+) or opposite (-) direction of the natural helicity of the cord, changing the coiled state of the cord through torque. In this example, the DNA is the telephone cord while the handset is the magnetic bead. Instead of our own hand pulling upwards, the magnetic field attracts and/or orients the bead.

The magnetic field is usually oriented parallel to the surface to which the tether is immobilized and the magnitude of the magnetic field decreases with distance from the magnet. This creates a field gradient such that an attractive force is generated according to

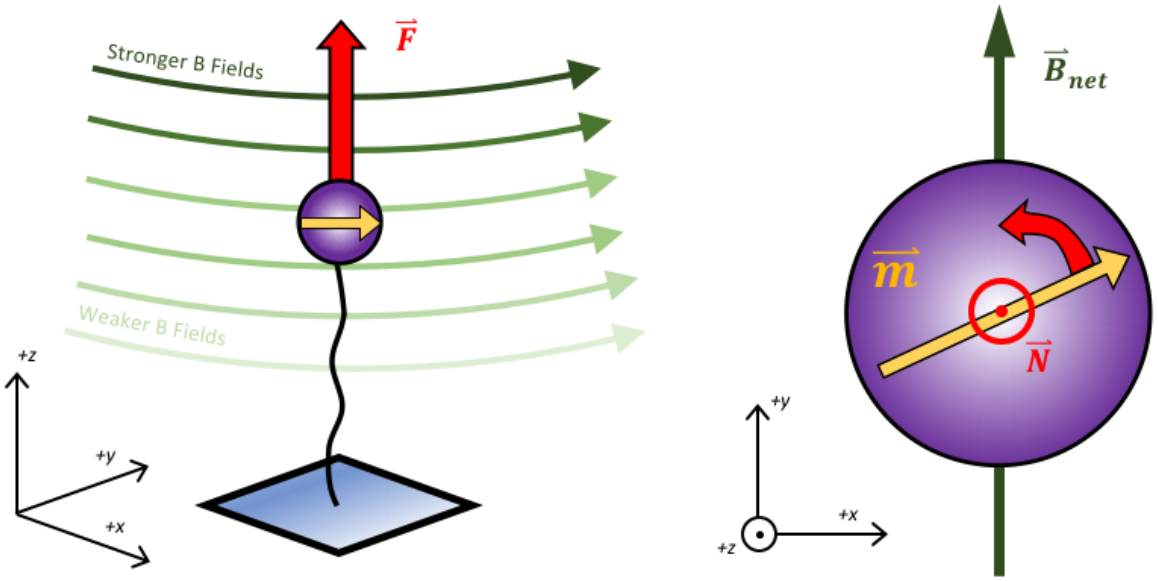

Figure 5: Magnetic Bead Field Interactions - A molecule of DNA (black line) is shown immobilized to a glass surface (blue) and attached to a magnetic bead (purple). The magnetic moment of the bead is shown as a yellow arrow. The source of the magnetic field (not pictured) is located above the tether in the +z direction. **Left-** To generate attractive force, the B fields (green arrows) decrease in magnitude away from the source (-z direction). This field gradient along with the magnetic moment's tendency to align with an externally applied field causes the attractive force (red arrow). **Right-** Top-down view. To generate torque the net magnetic field (green arrow) must be rotated along the xy-plane. After a direction change, a brief period of magnetic moment misalignment occurs. During this interval, a torque (red arrow) is applied until the magnetic moment realigns. If the B field is continuously changed along the xy-plane in a clockwise (CW) or counter-clockwise (CCW) fashion, turns are introduced into the DNA tether. These turns change linking number, therefore allowing the supercoiling of DNA.

$$\mathbf{F} = \frac{1}{2}\nabla(\mathbf{m} \cdot \mathbf{B}). \quad (6)$$

The magnetic force is given by $\mathbf{F}$ (N), the magnetic moment of the bead by $\mathbf{m}$ (A*m^2), and the external magnetic field by $\mathbf{B}$ (T).[11] Furthermore, the field can also be manipulated 360° along the plane of the immobilization surface so that torque may be achieved according to

$$\mathbf{N} = \mathbf{m_o} \times \mathbf{B}, \quad (7)$$

where $\mathbf{N}$ (N*m) is the torque and $\mathbf{m_o}$ is the component of the magnetic moment initially not aligned with $\mathbf{B}$.[9] In equation (7), $\mathbf{B}$ is treated as a constant magnetic field at the particular distance from the magnet, as field strength varies negligibly along the plane parallel to the immobilization surface. A diagram of a DNA tether responding to an applied external magnetic field is given in Figure 5. Attractive force and torque constitute the two force regimes of MT.

The utility of magnetic tweezing lies in the capability to change DNA topology in real-time. This is especially relevant, because DNA is normally topologically constrained *in vivo* via tension and twist, conditions that were previously difficult for experimentalists to reproduce *in vitro*.[13,14] When attractive force is exerted on the bead, the DNA tether stretches like a telephone cord under tension. Furthermore, torque can be applied to add/subtract twists from the molecule, creating supercoiling. This mechanically introduced supercoiling can induce loop formation, shortening overall tether length.

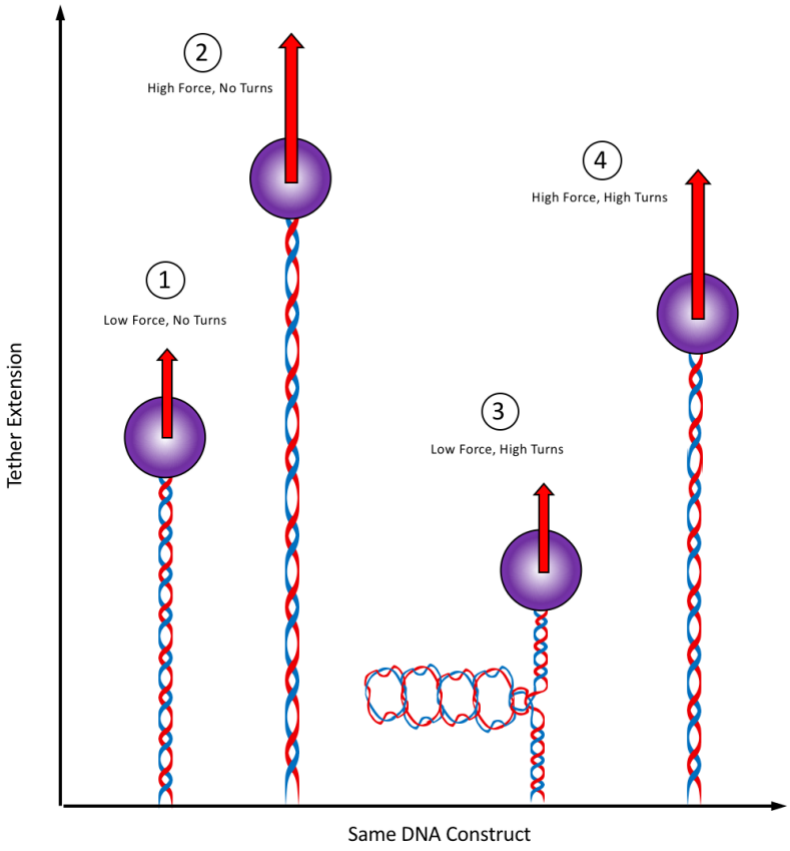

Figure 6: Magnetic Tweezer dsDNA Manipulation: Different conformations of dsDNA can be induced through attractive force and torque. If attractive force is increased, the DNA double helix can be stretched along its vertical axis (1 to 2). In this dimension, the pitch of the DNA increases. Under constant lower forces (< 1 pN), turning the dsDNA by applying torque supercoils the double-helix. Supercoiling induces loop formation, which reduces the tether length (3). Plectonemic loops are shown in this figure. In ssDNA, turning does not affect supercoiling because the strand can rotate about the phosphate backbone made from single-bonds. By contrast, dsDNA's hydrogen bonding along its internal vertical axis prevent this single-bond spinning. If force is increased in a highly supercoiled molecule, the writhe of the DNA converts to twist as the DNA loops are 'pulled out' (4).

The effects of tension and turns on tether extension are shown in Figure 6. Furthermore, the interactions of TFs and other DNA-binding proteins with DNA can alter the effective tether length under certain force and torque conditions. These two force regimes have been used to investigate the effects of DNA topoisomerases[15], helicases[16], and RNA polymerase[17] on DNA mechanics, contributing to our understanding of their respective mechanisms.

Traditionally, magnetic fields have been applied via permanent rare-earth magnets positioned above the DNA sample. The field is modulated by physically moving the magnets using motorized mechanical translators. This mechanical setup is shown in Figure 7. Although this technique applies the necessary magnetic forces on each strand, the motor's mechanical motion introduces vibrations into the experimental system which interfere with accurately tracking the bead to measure tether length and force. Moreover, the applied field strength cannot be changed instantaneously, nor re-oriented quickly to release rotational constraints; therefore, experiments involving step-response measurements are difficult to realize. The fact that the B field of permanent magnets can only be manipulated via direct motion is a major weakness for applications that are sensitive to vibrations, like microscopy. To create a

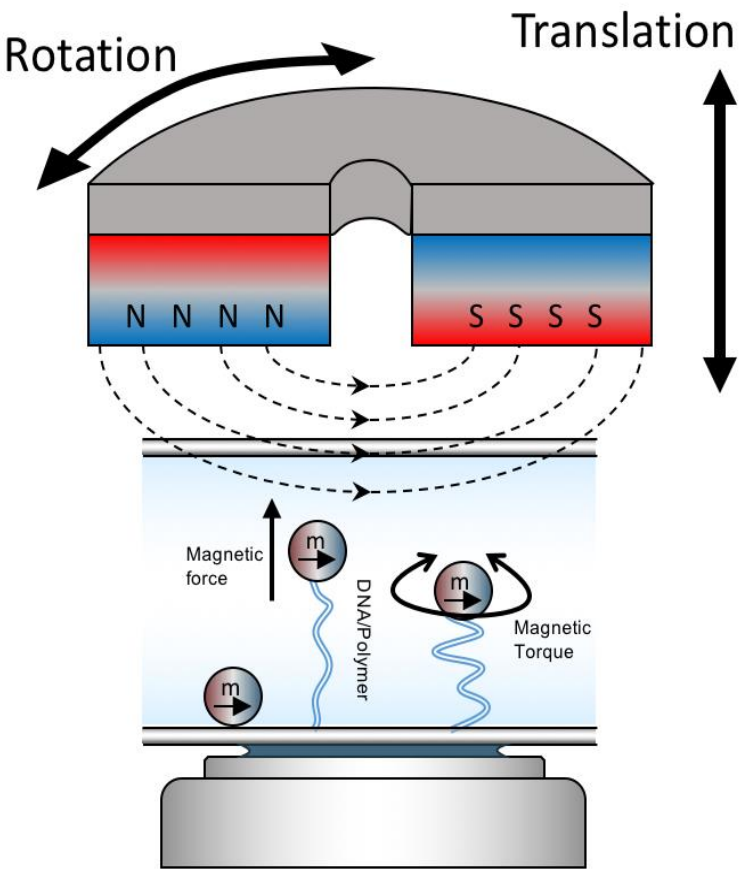

Figure 7: Permanent Magnetic Tweezer Overview - In traditional magnetic tweezers, a rare earth metal magnet generates a magnetic field between its north and south poles. Attractive force and torque are achieved through the manipulation of the B field, which in a permanent magnet system requires changing the position of the metal magnet with respect to the sample. The permanent magnet is translated vertically and rotated to modulate attractive force and torque, respectively.

solid-state system that is both more dynamic and mechanically stable, current carrying wires can be employed to generate the desired magnetic field.

E. Solenoid Magnetic Fields

A solenoid is a current carrying wire arranged in a coil structure. This coiled structure is typically wrapped around a cylindrical shape, which in commercial applications is some material with magnetic properties. Materials may be paramagnetic or diamagnetic, meaning they acquire a magnetization parallel or antiparallel, respectively, to an external magnetic field. Perfectly paramagnetic or diamagnetic materials only magnetize when an external magnetic field is applied.

Elementary electrodynamics may be used to describe the magnetic field generated by a solenoid wrapped around a magnetizable material.[18] Ampere's law may be used to calculate the magnetic field generated by a current. The integral form of Ampere's law is

$$\oint \mathbf{B} \cdot \mathrm{d}\mathbf{l} = \mu_0 \mathrm{I}_{\mathrm{enc}} \tag{8}$$

where $\mathbf{B}$ (T) is the field generated, $\mathrm{d}\mathbf{l}$ is some infinitesimal segment of the amperian loop, μ_0 is the permeability of free space $\left(\mu_0 = 4\pi \times 10^{-7} \frac{N}{A^2}\right)$, and $\mathrm{I}_{\mathrm{enc}}$ (A) is the current enclosed within the amperian loop. This equation can be easily applied to systems in free space with no magnetic materials. In systems with materials able to magnetize, either paramagnetically or diamagnetically, the net magnetic field is affected by both free current and the material's magnetization properties. The relation between the material's magnetization $\mathbf{M}$ (T) and magnetic field $\mathbf{B}$ are expressed as $\mathbf{H}$, given by

$$\mathbf{H} = \frac{1}{\mu_o}\mathbf{B} - \mathbf{M}. \tag{9}$$

For a system with free currents and a magnetizable material, we can combine equation (9) and the integral form of Ampere's law to form

$$\oint \mathbf{H} \cdot \mathrm{d}\mathbf{l} = \mathrm{I}_{\mathrm{f,enc}}\,, \tag{10}$$

where $\mathrm{I}_{\mathrm{f,enc}}$ is the free current enclosed by the amperian loop. Materials whose $\mathbf{M}$ is directly proportional to $\mathbf{H}$ are known as linear media. In linear media, $\mathbf{M}$ and $\mathbf{H}$ are related by

$$\mathbf{M} = \chi_{\mathrm{m}}\mathbf{H}, \tag{11}$$

where χ_{m} is a dimensionless quantity describing the magnetic susceptibility of the material. By substituting equation (11) into equation (9), we find that

$$\mathbf{B} = \mu\mathbf{H} \tag{12}$$

where

$$\mu = \mu_o(1 + \chi_m). \tag{13}$$

The magnetic field generated by a solenoid coil wrapped around a magnetizable material can now be derived. To understand the basic concept of a solenoid generated field, an infinitely long solenoid and core will be assessed. This system is pictured in Figure 8. The two regions of interest are inside (s < R) and outside the coil (s > R), where s is the radial distance from the z axis. The z axis lies along the vertical axis of the cylinder. Using equation (10) for loop A, since $I_{f,enc}$ is 0, we find the following:

$$\begin{aligned} H(d)L - H(c)L &= 0 \\ H(d) &= H(c) = 0 \\ \mathbf{H}(s > R) &= \mathbf{0} \end{aligned} \tag{14}$$

This is because the horizontal sections of A do not contribute to the closed path integral of equation (10). Assuming the coils are essentially horizontal and magnetization is fully paramagnetic/diamagnetic,

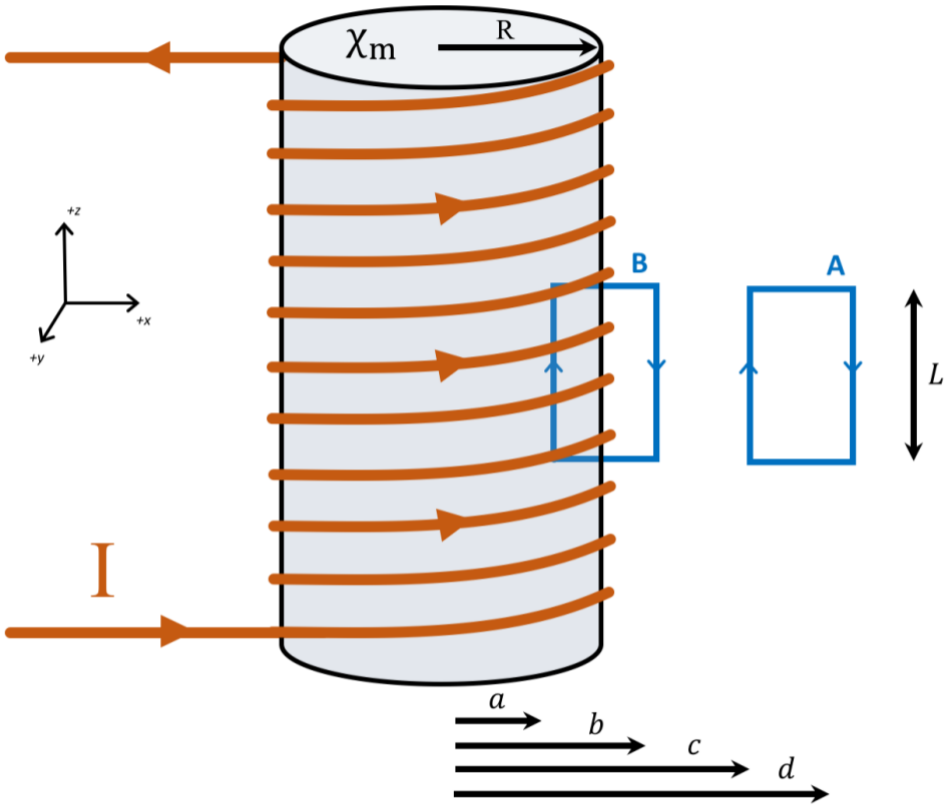

Figure 8: Derivation of Solenoid Magnetic Fields - A current carrying wire (orange) is wrapped around a core material (gray) with magnetic susceptibility χ_m and radius R. The wire and core form an infinitely long solenoid. The cartesian directions are shown by the axis on the left. In a cylindrical coordinate system, the z axis is along the central axis of the solenoid core with s pointing radially. The gaussian loops A and B (blue) have vertical segments of length L located at s of a, b, c, and d.

by the right hand rule, $\mathbf{H}$ is restricted to the z direction. The dot product for the horizontal sections is 0. Furthermore, we find that $\mathbf{H}$ is equal in magnitude at distances *c* and *d*. The only possible value of **H** that allows the field to approach 0 as *s* goes to infinity is 0.

Next, we evaluate loop B by equation (10) to find $\mathbf{H}$ within the solenoid where n $\left(\frac{\text{loops}}{\text{length}}\right)$ is the looping density of the coil, we find

$$\mathbf{H}(\mathrm{s} < \mathrm{R}) = \mathrm{nI}\,\hat{\mathbf{z}}\,. \tag{15}$$

We have this result because the only contributing segment of loop B to the line integral in equation (10) is at radial distance *a*. By plugging equation (15) into equation (12), we find that the generated internal magnetic field can be expressed as

$$\mathbf{B_{in}} = \mu_{\mathrm{o}}\mathrm{nI}(1 + \chi_{\mathrm{m}})\,\hat{\mathbf{z}}\,. \tag{16}$$

One important implication of equation (16) is that the magnetic field's magnitude and vertical direction can be manipulated by controlling current via a power supply. The value of χ_{m} is positive or negative based on whether or not the core material is paramagnetic or diamagnetic, respectively.[18] This means that using a paramagnetic core material enhances the internal magnetic field. Furthermore, using paramagnetic materials that extend beyond the solenoid coil allows us to focus the field in a particular direction. Multiple solenoid coils can be employed in an instrument to generate a net magnetic field by simple superposition.

II. Electromagnet Construction

A. System Overview

Three major inter-working components must be implemented to create an experiment-ready electromagnetic tweezer (eMT): electromagnet hardware, electrical hardware, and computer software. An overview of this system may be found in Figure 9. Beginning with the computer software, the user interacts with a custom graphical user interface (GUI) designed to control a MATLAB script. This user interface allows the user to control the magnetic field strength (attractive force) as well as the angle of the field (torque) on a sample located below the electromagnet hardware. The MATLAB program then interacts with the device driver, a program in direct communication with the electrical hardware. On our board, the commercially available microcontroller utilizes user issued commands to regulate 2 current controllers. Each current controller diverts specified amounts of electrical current from the DC power supply to a pair of solenoid coils wired in series on the electromagnet hardware. The electromagnet consists of 4 solenoid coils arranged vertically on the four corners of a square frame, wherein the coils on opposing corners are wired in series. An overview of the magnet configuration and field generation

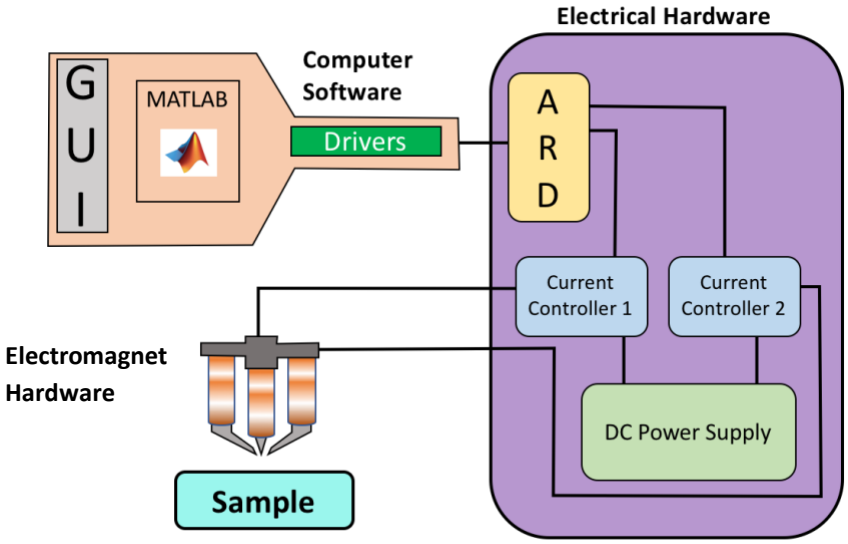

Figure 9: Magnetic Tweezer Development Overview - Three aims of development had to be achieved to create a contemporary, user-friendly instrument for the study of single-molecule systems. Beginning with computer software, a GUI must manage user commands in Matlab and communicate with device drivers. These drivers interface with the second aim of development, electrical hardware. The electrical hardware integrates user-commands to directly manage a DC power supply. Using two current controllers, the electrical hardware dictates the voltages across each set of solenoid coils in the third developmental aim, electromagnet hardware. The electromagnet hardware is made up of the solenoid coils and frame mounted to the magnetic tweezer microscope. The electromagnet hardware is mounted directly above the sample.

can be found in Figure 10. The program utilizes user input to manipulate the electrical current through each pair of solenoid coils, resulting in 360° possible B field generation along the plane below the electromagnet. The ability to change the magnitude and direction of the net B field through current manipulations allows one to exert attractive forces and torque.

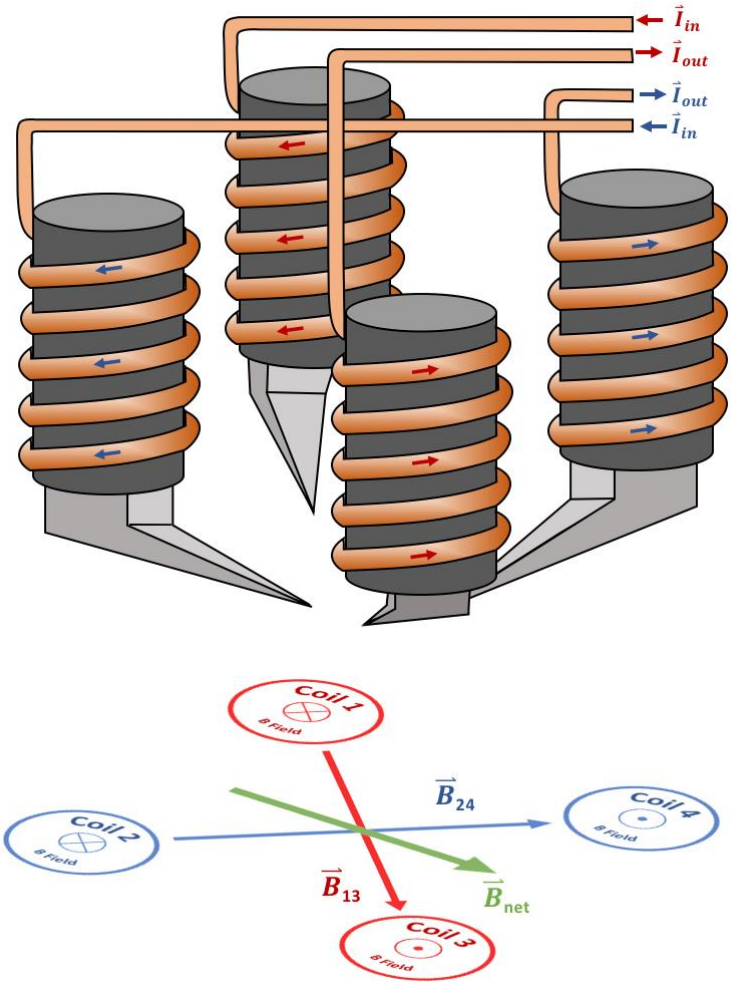

Figure 10: Electromagnet Hardware and Generated B Field - The electromagnet hardware consists of 4 solenoid coils arranged in a square formation. The coils on opposite corners are wired in series such that the field generated by each solenoid follows a circular path along the pole pieces below. This occurs because the magnetized materials within each solenoid apply a B field to the materials beyond the wiring. The magnetizable pole pieces 'pass on' magnetization from the coils to the pointed end. Each pair generates a field below (red or blue arrow) whose magnitude can be manipulated by controlling current magnitude and direction. Due to the mutually perpendicular directions of each pair's magnetic field, a net magnetic field (green arrow) can be produced in 360° by superposition.

B. Frame and Solenoid Construction

Implementing the electromagnetic tweezers required the production of four custom solenoid coils mounted in line with the microscope axis (Figure 11). For this task we employed the services of the machine shop within the Department of Physics. The digital design and schematics of the electromagnet frame were produced using Fusion 360 (San Rafael, CA), an Autodesk computer-aided design (CAD) software. The main structure consisted of an outer frame composed of low carbon steel mounted on a central aluminum section. Each solenoid consists of 460 turns of magnet wire (CNC Tech PN 60022) wound around a steel core. An octahedral pole-piece protrudes downwards from each solenoid coil to focus the generated field directly above the sample stage. By tightly confining the field, high forces can be achieved even if the overall field strength is low. Prior to manufacturing, we modeled the performance of the quad-pole electromagnet design using two finite element packages: the commercial CST Studio (CST of America, Inc. Framingham, MA) package and the open-source ElmerFEM maintained by CSC – IT Center for Science. The computer modeling results guided the geometric scale of the instrument. Both simulation tools suggest that the gradient of the electromagnet is comparable to that of previously used permanent magnetic tweezers.

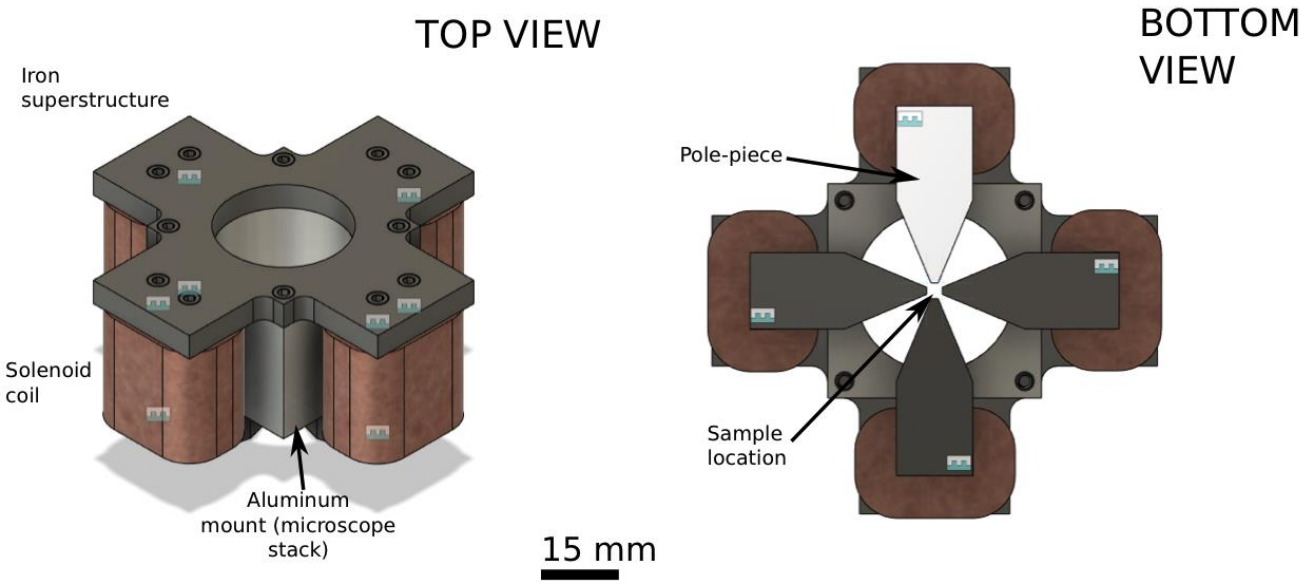

Figure 11: Electromagnetic Tweezer Frame Schematic – Both views were generated in Fusion 360. Dark grey represents low carbon steel while the light gray represents aluminum. The scale above is 15 millimeters. **Left-** Top view of the electromagnetic tweezer frame with different sections labelled. **Right-** Bottom-up view of the electromagnet. The octahedral pole-pieces, all made from the same low carbon steel, are clearly shown protruding from each solenoid. The pointed ends reach toward the center to help focus the field gradient, improving the applied attractive force and torque. The light source shines through the circular passage and the small gap in the pole pieces.

C. Electrical Hardware

Prototyping was an important dimension of developing the electromagnet. Because we were developing experimental electrical hardware, an inexpensive, time-efficient, and mistake-friendly way to produce custom circuit boards was required. Each printed circuit board (PCB) began with a digital design. Early prototyping used Eagle CAD to layout the electrical parts of the circuit on a digital board. To be translated from the computer to an analog board, the Eagle design was then exported to AutoCAD. AutoCAD converted the original design to a pdf file for etching onto a copper-clad board by a laser cutter (Universal Laser Systems VLS460).

The laser cutter translated the digital design of the circuit board onto copper clad board. This translation, however, occurred in three major steps. First, the copper clad board was spray-painted with ACE Gray Paint Primer 17031. This spray paint was then etched off according to the AutoCAD pdf during laser cutting. The entire board was then placed in 200 mL of 1 M hydrochloric acid (EMD B07061; CAS 7647-01-0) and 5 mL of hydrogen peroxide (Sigma-Aldrich MKBH9385V; CAS 7722-84-1). The exposed portions of the copper board were removed during this acid bath. This copper removal process is shown in Figure 12. Following a 10-minute period, the board was examined visually every 2 minutes to ensure over-etching did not occur. After the acid bath, the leftover paint primer was removed using acetone (Sigma-Aldrich; CAS 67-64-1). Following a drying period, a coat of ACE Purple Gloss 1066422 was applied to all of the sections of the board excluding where electrical contacts were intended. Next, holes were drilled on all through-hole pads using a Dremel 3000 Variable Speed Rotary Tool mounted on a Prozone PZ541 Drill Stand. The entire PCB fabrication process is pictured in Figure 13.

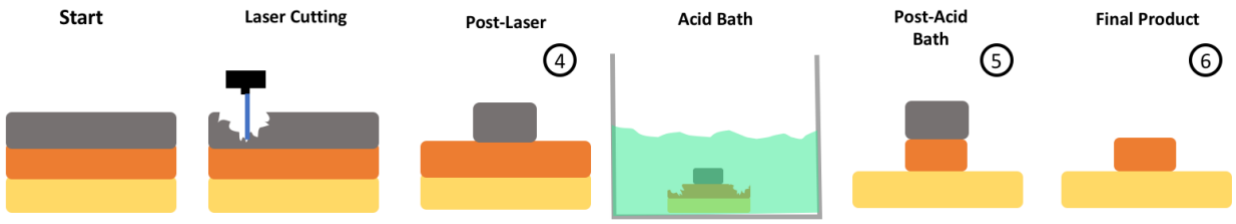

Figure 12: Prototype Board Layering - The process of creating homemade printed circuit boards relied on the differential layering of an initial board, consisting of paint primer (gray), copper (orange), and fiberglass (yellow). A laser cutter removed undesired segments of primer (4) followed by an acid bath to remove the exposed copper regions (5). A nonpolar solvent would then be used to strip the remaining paint primer to reveal the predetermined copper electrical leads (6). The numbering above each step corresponds to the pictures in Figure 13.

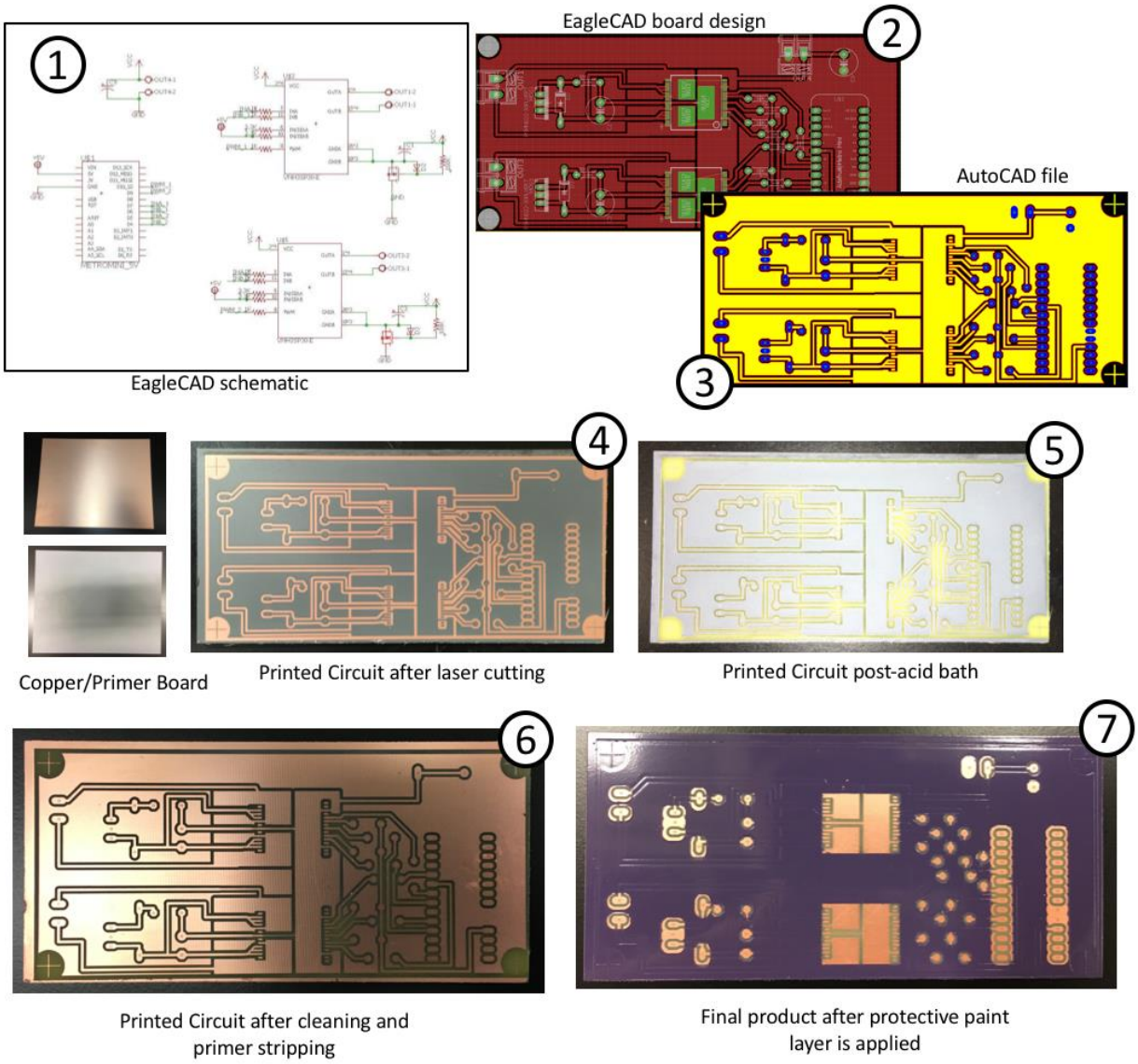

Figure 13: Circuit Board Prototyping Stages – (1) Beginning with an overall circuit schematic in Eagle, the electrical components were planned. The schematic was then translated to a circuit diagram (2) that outlines the physical dimensions and position of each electrical component. This design was then exported to AutoCAD for conversion to a color-coded, properly scaled pdf (3) compatible with the laser cutter. The design was etched into the painted copper clad board (4) and then treated in an acid bath (5). Following this, the paint was stripped by a nonpolar solvent (6) and paint was applied to non-soldering areas to provide thermal shielding (7).

Following PCB fabrication, the next step in developing prototype circuits was attaching electrical components. The first of two soldering phases was to attach the surface mount current controllers using ChipQuik TS391SNL50 Thermally Stable Solder Paste. Surface mount soldering (SMS) is utilized in industrial circuit board fabrication because it is efficient and automatable. Instead of using a soldering iron and solder core, SMS is performed by spreading a solder paste to desired areas and heating the

entire board along a manufacturer-specified heating curve. Solder paste has a peanut butter-like consistency made from microscopic solder fragments suspended in a carrier oil. During heating, the carrier oil evaporates and the solder melts to create solid contacts. The heating curve's shape exists to avoid electrical component damage from prolonged high-heat exposure. Typically a commercial reflow oven is used to achieve the proper heating curve, however we did not have access to one. Instead, we built our own reflow oven by modifying a conventional toaster oven to include a thermocouple, logic-controlled relays, and custom MATLAB software to control heating. This custom reflow oven and heating curve are shown in Figure 14. Following a cool-down, the through-hole components were attached using a Weller Model WLC100 40-Watt soldering iron and RadioShack 0.22" 62/36/2 Rosin Core Solder.

The prototype boards were tested using a power supply and the electromagnet hardware. We verified that the hardware was able to drive currents through the electromagnet coils using pulse width modulation (PWM) and that the resultant magnetic field could manipulate paramagnetic beads. The 'homemade' electrical hardware fulfilled its essential role to generate magnetic fields, however excessive amounts of heat were produced during prolonged use. To combat this issue, a multi-layered

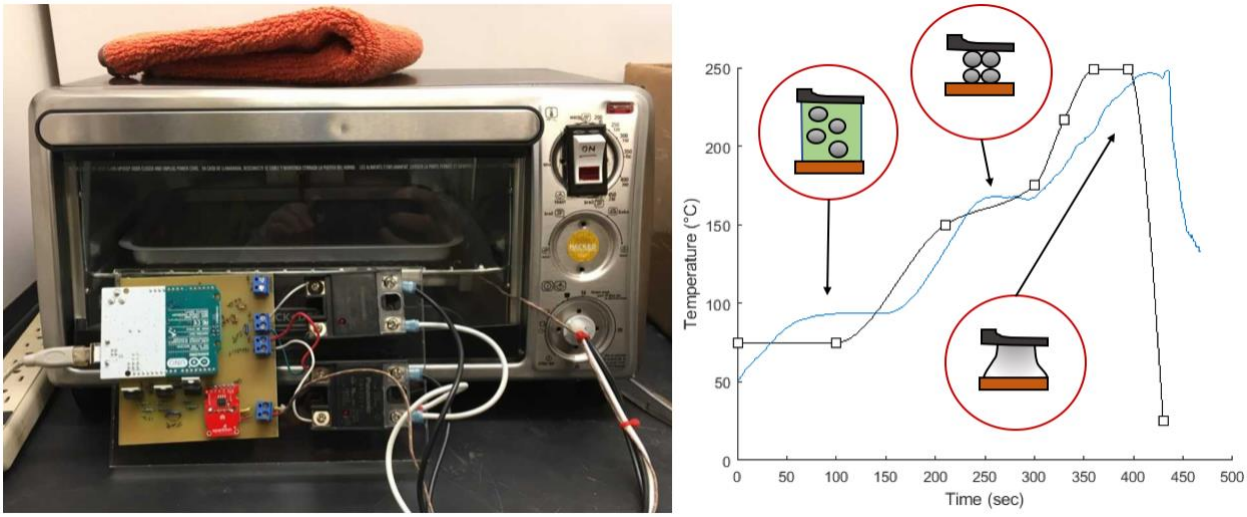

Figure 14: Reflow Oven Overview – **Left-** A conventional toaster oven was stripped of its original components and a custom circuit was made to allow for heating along a specific curve. A thermocouple for measuring temperature in real-time was added along with 2 heavy duty relay switches to control the 2 heating elements within the oven. An Arduino microcontroller managed these electrical components using a custom Matlab script connected via USB. **Right-** A manufacturer-specified heating curve (black) establishing temperature intervals was input to the Matlab program. The solder carrier liquid evaporates during the intermediate temperature interval, followed by the solder melting to form solid electrical connections. When the temperature read by the thermocouple was lower than the goal set by the curve, the relays switched on and provided current to the heating elements. When temperature exceeded the goal temperature, the relays shut off. The temperatures achieved in real-time (blue) properly soldered the current controllers to the board.

design for professional production was made, keeping the electrical component superstructure largely the same. Using KiCAD, an open-source electronic design application, we designed a four-layered circuit to assist in thermal management. Two layers of this board operated exclusively to dissipate heat, consisting of large copper pours and thermal vias. These multi-layered design aspects are difficult to manufacture in-house so production was outsourced to a professional fabrication facility (Advanced Circuits). With the multi-layered board in hand, the previously-described reflow oven and through-hole soldering were used to complete the electrical hardware. The circuit was then housed in a clear plastic casing to prevent the shorting of electrical components and to improve cable management. This final circuit board was used for biological testing. The final electrical hardware product is shown in Figure 15.

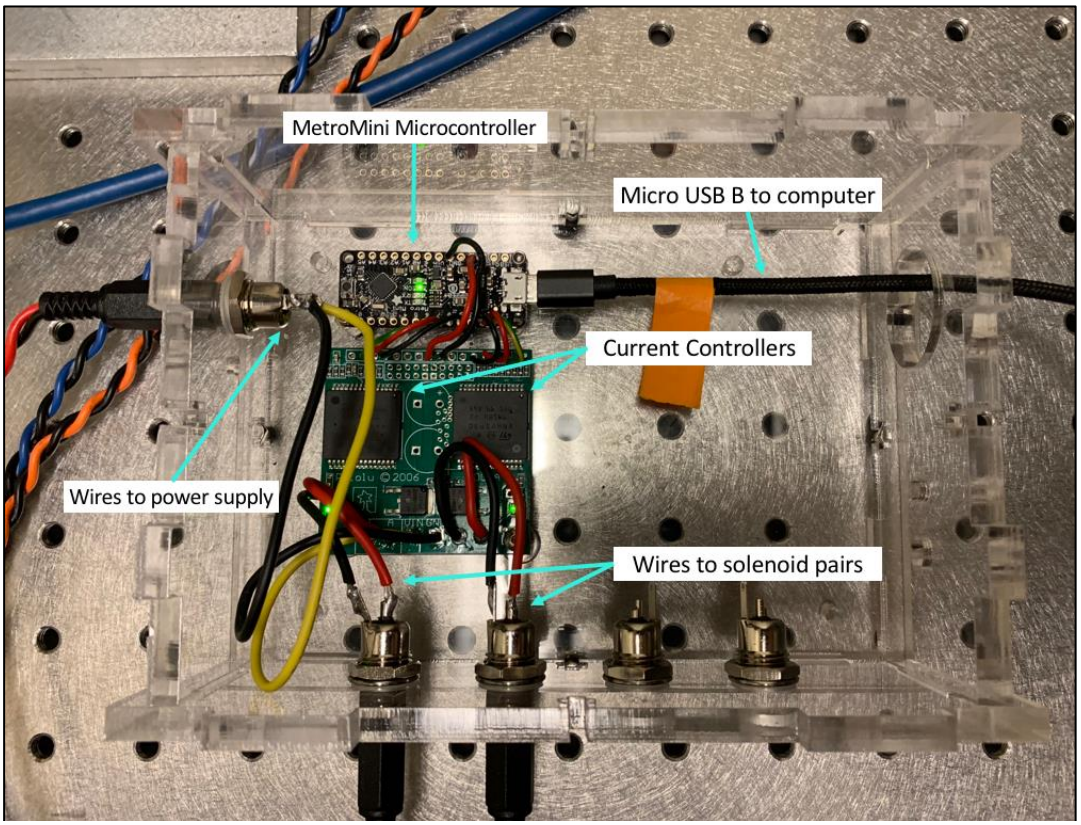

Figure 15: Electrical Hardware Final Product - The final electrical hardware setup consisted of a professionally fabricated board and MetroMini microcontroller. This microcontroller is similar to an Arduino and interfaces with the commanding computer via USB B. The microcontroller uses PWM to dictate voltage settings on each current controller. The voltage is provided by an external DC power supply. Each current controller channel is wired to a solenoid pair via the blue/black and orange/black wires.

D. Computer Software and Interface Structure

In order to fully integrate the electromagnet into single-molecule experiments, the magnetic field direction and magnitude must be easily controllable by an experimenter without advanced training. This user-friendly aspect of the electromagnetic tweezers was accomplished by making a GUI. Made by Dr. Dan Kovari and Dr. Josh Mendez, this GUI (Figure 16) allows the user to specify the magnitude and direction of the generated magnetic field. The 'Turn Controller' portion of the GUI can manipulate the field in a curvilinear manner along the plane of the microscope stage. The magnetic field manipulations made possible by the GUI can be macroscopically visualized using a compass, displayed in Figure 17.

The overall command structure for the electromagnet begins with the user and ends with the magnetic field produced. The GUI communicates with a microcontroller via USB to control the magnitude and direction of the current through the solenoids. As noted above, control of the coil current is achieved through an intermediary driver board which takes a pulse-width modulation (PWM) signal from the microcontroller and translates this signal into an effective power delivered to a coil pair. An additional digital flag (5V or 0V) specifies the direction of current flow through the coils.

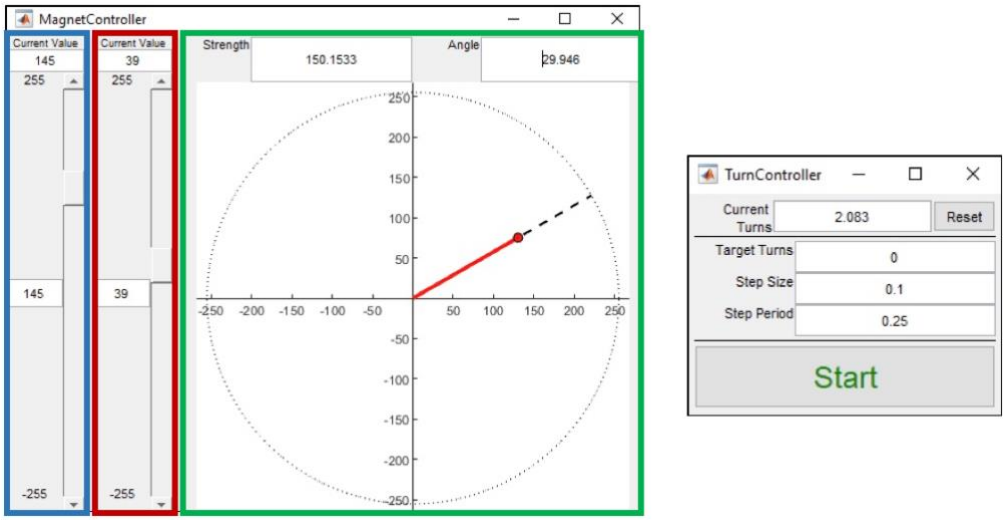

Figure 16: Graphical User Interface (GUI) – **Left-** The magnet controller is used to intuitively specify a field direction and magnitude. The PWM values for each respective solenoid pair are shown in the blue and red boxes. These individual B fields superimpose to create the net B field shown in the green box. The fields for current value, overall strength, and angle are all adjustable. Additionally, the red slider is directly manipulated using the mouse to change field strength and angular orientation. **Right-** The turn controller allows the user to spin the magnetic field by issuing specific turn commands, which include specifying a target turn value, step size, and step period.

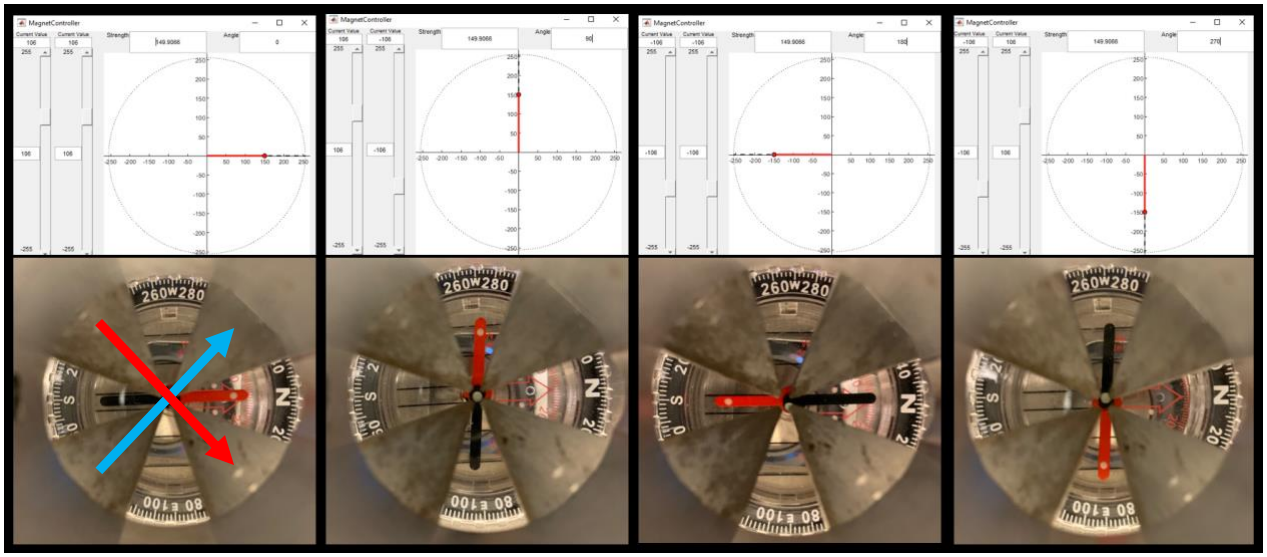

Figure 17: Visualization of Graphical User Interface Commands - This figure shows an electromagnet GUI setting and the resultant B field visualized macroscopically by a compass. Each picture was taken down the central axis of the electromagnet frame in between solenoid arrangement. The pole pieces block certain parts of the compass. Notice the orientation of the red arrow in the GUI. When the B field angle is set to 0°, the compass points to the right. The blue and red arrows show the field generated by each solenoid pair. These two components superimpose to create the net field direction shown on the compass. When the B field angle is set to 90°, the compass needle points upwards. This pattern is continued for angle settings 180° and 270°.

III. Experimental Planning

A. DNA Sample Preparation

In order to test the electromagnet's single-molecule experiment capabilities, microscope flow-chambers were assembled with solutions containing super-paramagnetic beads tethered by single dsDNA molecules to the surface of the chamber. A number of microbiology techniques were used in order to prepare such samples. The primary techniques used were polymerase chain reaction (PCR), specific cleavage/ligation by enzymes, and gel electrophoresis.

PCR is used to produce a large number of copies of a particular sequence of dsDNA. First, ssDNA is obtained by melting dsDNA at high temperatures. High temperatures disrupt the hydrogen bonds along the DNA double-helical axis. This produces 2 strands of complementary ssDNA. These strands are then slowly cooled to an annealing temperature (50-56°C) where DNA polymerase activity is low, during which primers can bind to each ssDNA. Primers are short oligonucleotides complementary to one end of the DNA template. The whole mixture can then be heated to 72°C, at which DNA polymerase's binding

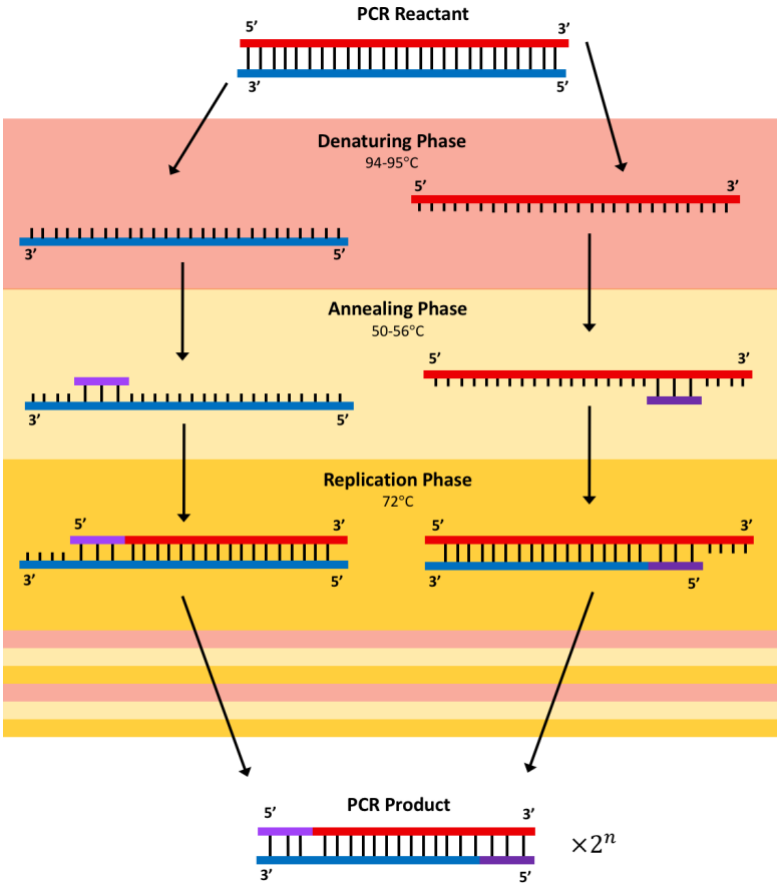

Figure 18: Polymerase Chain Reaction - In PCR, parent dsDNA is denatured to form two complementary ssDNA segments at high temperatures. After slowly cooling to an annealing temperature, primers in solution hybridize to complementary regions. After a time interval, the entire solution's temperature is raised to favor DNA replication. DNA polymerase in solution binds to the primers and replicates DNA in the 5' to 3' direction. This full cycle is repeated many times to amplify the DNA segment between the primers. Once significantly more nascent DNA exists in solution, primers will mostly bind to DNA that contains the sequence only to the antiparallel primer.

activity increases. Once bound, DNA polymerase incorporates dNTPs from the solution into new phosphodiester linkages to extend the primer in the 5' to 3' direction. As the solution cycles through these three temperatures, the dsDNA sequence in between the two primers is amplified in an exponential fashion.[19] To functionalize DNA molecules for specific binding, the dNTPs used in solution may be individually modified to include biotin or digoxigenin.[12] An overview of PCR is shown in Figure 18.

The second important microbiology technique used was cleavage and ligation by restriction enzymes and ligases, respectively. In prokaryotic genomics, restriction enzymes recognize specific sequences of DNA and cut the phosphodiester linkages nearby. Some enzymes may cut palindromic or non-palindromic sequences. A palindromic sequence is a segment of dsDNA that contains the same 5' to 3' base pair order on the opposing single strands of DNA. Restriction enzymes produce blunt or overhanging cuts in DNA. In our experimentation, we used restriction enzymes that produced a ssDNA

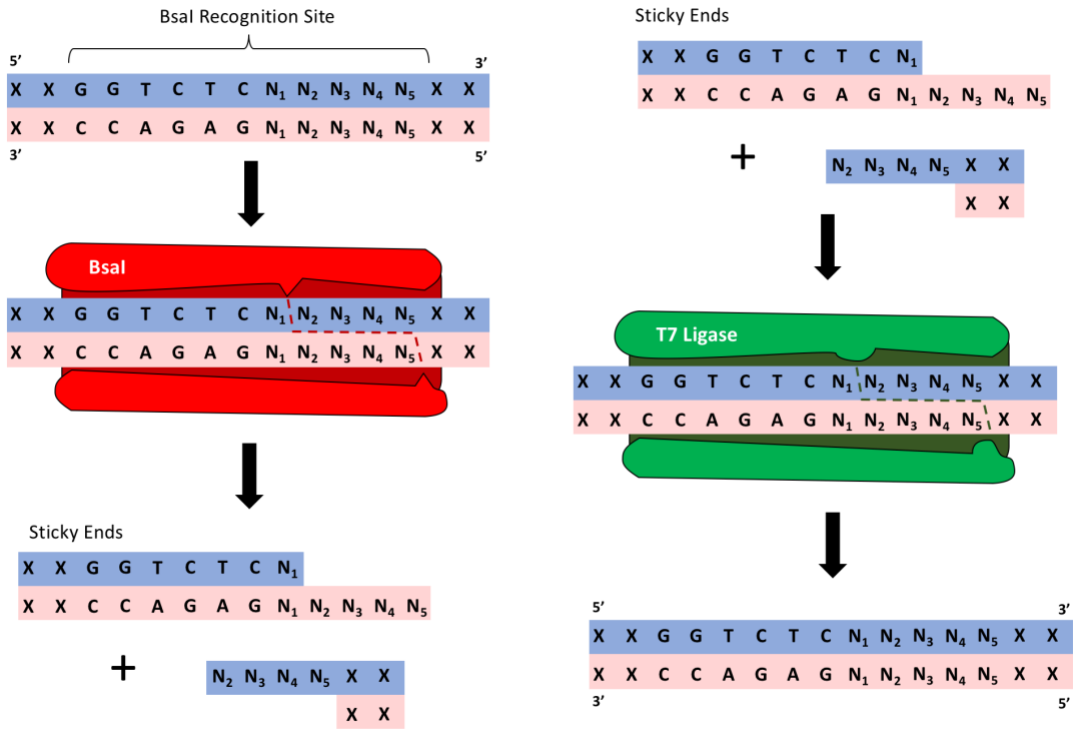

Figure 19: Restriction and Ligation Enzymes - dsDNA sequences (red and blue) are shown containing regular nucleotides like A T, G, and C as well as variable base pairs denoted by N values. The X values outside of the recognition sites/overhangs are also variable base pairs but are uninvolved in enzymatic actions. **Left-** The restriction enzyme BsaI acts by recognizing a particular sequence and then cutting it in a non-palindromic fashion. This cut also produces sticky ends. **Right-** Sticky ends of the BsaI recognition site are attached by T7 ligase nonspecifically to produce a single dsDNA.

overhang. These overhangs form ‘sticky ends’ that can be efficiently reattached to other complementary sequences by enzymes called ligases. An overview of restriction and ligation can be found in Figure 19.

Gel electrophoresis is a common method used to verify the products of PCR, restriction, and ligation reactions.[20] When agarose and water are mixed, a hydrogel is formed. This hydrogel has nanometer scale pores that allow for DNA to ‘slither’ through.[21] DNA, which has an overall negative charge due to the phosphate backbone, can be pulled through an agarose gel by an applied electric field. Smaller DNA molecules incur less resistance when passing through the gel pores and as a result travel farther than their larger counterparts in the same amount of time. In a gel electrophoresis experiment, DNA samples are compared with a stock sample of assorted DNA lengths, known as a ladder. An overview of gel electrophoresis can be found in Figure 20.

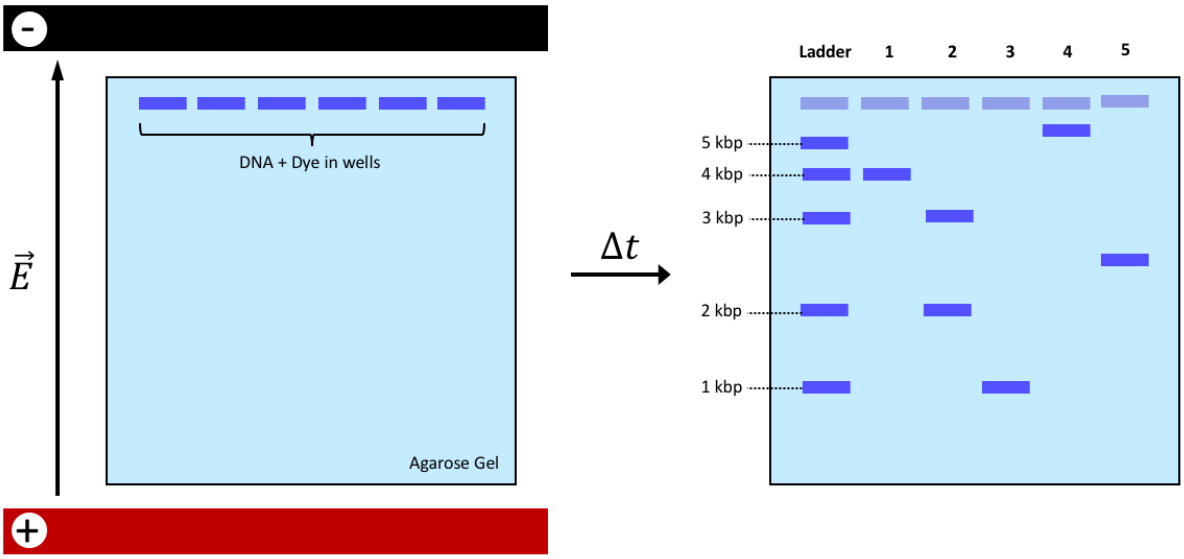

Figure 20: Gel Electrophoresis - An agarose gel containing various DNA-dye mixtures is placed in an electric field. After some time interval, the gel is removed from the electric field for analysis. In the leftmost lane, a DNA ladder with known base pair sizes creates a standard for comparison with the experimental DNA lanes. In this gel, we would conclude that the DNA sample in lane 1 is about 4 kbp. We would conclude that lane 2 contains two separate DNA molecules of 3 kbp and 2 kbp. We would conclude that the DNA in lane 3 is approximately 1 kbp. For lane 4, the DNA would be suspected to be larger than 5 kbp. Finally, we would project that lane 5’s DNA sample is between 3 kbp and 2 kbp.

A custom DNA plasmid (pDD_IN2BbvCI) was used to create the biotin tail, main fragment, and digoxigenin tail portions of the DNA construct. This custom plasmid was constructed using several naturally occurring sequences from *E. coli*. The full sequence of the custom plasmid can be found in Appendix A. All three of the DNA fragments were made from different aliquots of pDD_IN2BbvCI. The specific primers, individual reaction schemes, and gel electrophoresis results can be found in Figure 21. To create the main fragment, a PCR with normal dNTPs was conducted using primers 1 and 2. For the biotin tail, a PCR between primers 3 and 4 spiked with biotin labelled deoxy-uracil triphosphate (Bio-dUTP) was used. For the digoxigenin tail, a PCR between primers 5 and 6 spiked with digoxigenin labelled deoxy-uracil triphosphate (Dig-dUTP) was used. During the tail PCR reactions, Bio-dUTP and Dig-dUTP are incorporated into growing DNA segments randomly in place of a low percentage of thymine. As a result, the tail segments are functionalized at different points along their length.

The agarose gel in Figure 21 shows the results of each PCR reaction. The bands in the gel show that the biotin and digoxigenin PCR reaction products had a length between 700 and 800 bp. The digoxigenin sample (796 bp) travelled a slightly shorter distance than the biotin sample (725 bp), confirming their length difference. The main fragment samples travelled slightly farther than the 4000

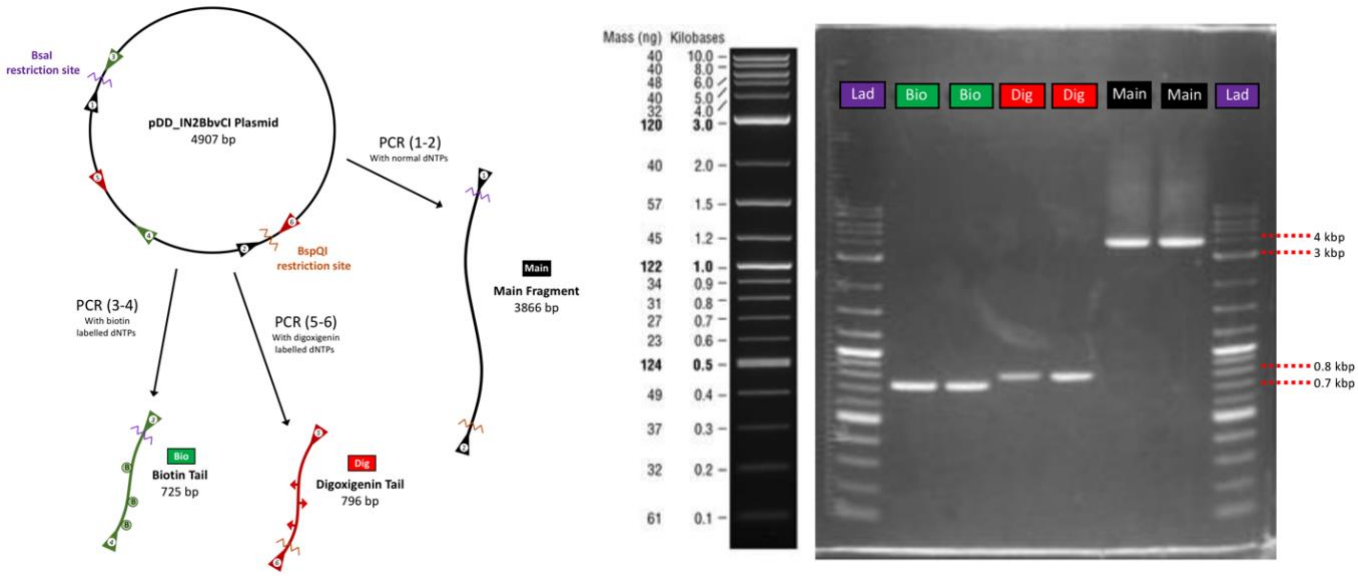

Figure 21: DNA Fragment Synthesis – **Left-** An overview of the pDD_IN2BbvCI plasmid is shown with each primer and direction labelled. Each fragment was synthesized in separate aliquots with different PCR reactants. The primers 1-6 are as follows: A/pDL2317/4536, A-pUC19-715, A/pZV/4900, S-pDD_1N-3234, A/pUC19/1440, S-pDD_1N-2811. The results of these individual PCR reactions were then verified using gel electrophoresis. **Right-** Results of gel electrophoresis using 1.5% agarose gel with 1.5 µL of 10 mg/mL ethidium bromide (EtBr) and 250 mL TAE running buffer. An identical DNA ladder, with the lookup table shown, was run on both sides of the gel. Ladder bands of interest are highlighted.

bp ladder band, confirming the anticipated length of 3866 bp. The next step was to create sticky ends on these fragments using the restriction enzymes BsaI and BspQI (New England BioLabs).

After assembling the main fragment and tails, these isolated DNA fragments needed to be combined using restriction and ligation. The restriction enzymes (BsaI and BspQI) used in our protocol cut non-palindromic recognition sites leaving overhangs. This type of restriction was chosen, because only the desired strands for attachment would possess complementary overhangs. Following digestion by restriction enzymes, T7 ligase (New England BioLabs) was used to combine the 3 dsDNA segments. T7 ligase, a non-specific ligation enzyme, reestablished the phosphodiester linkages to form the final dsDNA construct. An overview of this reaction as well as the gel electrophoresis results are shown in Figure 22. After confirming the DNA ligation products, the final DNA construct was isolated from the gel and was ready for introduction into flow-chambers.

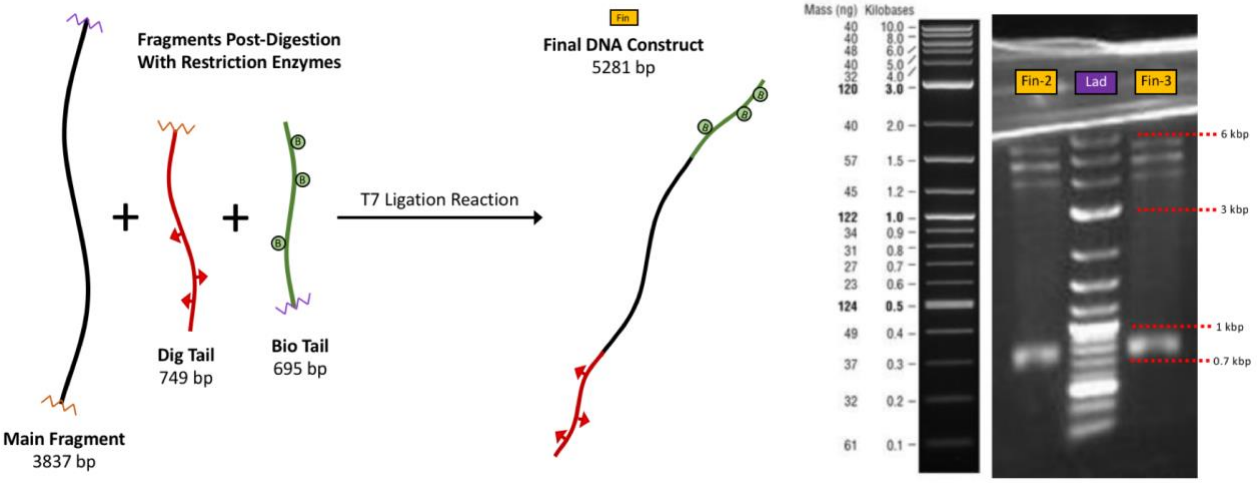

Figure 22: Final DNA Construct Assembly **– Left-** An overview of the ligation reaction to produce the final DNA construct is shown. The BsaI (purple) and BspQI (orange) overhangs were produced after enzymatic digestion. These three fragments were then combined together using T7 ligase to create the final DNA construct. **Right-** Two different DNA ligation reactions are shown in this gel electrophoresis experiment. The ratio of main to tail fragments was 1:2 in Fin-2 and 1:3 in Fin-3. This experiment used 1.5% agarose gel with 1.5 µL of 10 mg/mL EtBr. The concentration of TAE running buffer was too low and the gel folded during the experiment, however the bands of interest are still visible. The bands between 5-6 kbp represent the 5281 bp final DNA construct. Some smaller bands are visible at approximately 4.8 kbp and 4.1 kbp, most likely the result of unintended ligations of nonspecifically digested tails and main fragments. A large smear between 0.7 kbp and 1 kbp is visible, representing the unused reactants of the ligation.

B. Flow-chamber Preparation

The flow-chambers were made from a cleaned 24x50 mm coverslip (Fisher Scientific, Waltham, MA), a 22x22 mm square coverslip (Fisher Scientific, Waltham, MA), and a laser cut piece of parafilm sandwiched between. The flow-chambers were then heated on a hot plate until the parafilm became tacky and stuck to the glass on both sides. The clean, empty flow-chamber would then be ready for solution introduction and functionalization.

The solutions used during sample preparation served different roles. Phosphate buffered saline (PBS) pH 7.4 serves as a general purpose solution due to its similarity to biological pH and osmolarity for various cellular systems. Bead wash buffer (BWB) consists of 1 M NaCl, 10 mM Tris-HCl, and 1 mM ethylenediaminetetraacetic acid (EDTA). Tris-HCl is used as an effective buffer for biological pH while EDTA is used as a chelating agent. EDTA removes metal ions from solution, effectively inactivating DNA structure-compromising enzymes who rely on divalent metal ions to function.[22] BWB is used to clean and separate the magnetic beads for DNA attachment because the beads in stock solution frequently clump. Tethered bead buffer (TBB) consists of 100 mM NaCl in 20 mM Tris-HCl and 1 mM EDTA. TBB, which includes a typical nuclear salt concentration, was used for rinsing chambers during functionalization. Finally, stretching buffer (SB) consists of 100 mM NaCl, 0.2 mg/mL casein, 2 mM EDTA, and 0.5% volume per volume Tween in 20 mM Tris-HCl. Casein and Tween are used to prevent the nonspecific binding interactions of DNA and various proteins.[23]

After flow-chamber assembly, each cavity was rinsed with PBS and incubated with 4 μg/mL anti-digoxigenin (Roche, Madison, WI) in PBS for 1 hour. After incubation, each chamber was rinsed with TBB. The stock magnetic bead solution (Dynabead MyOne Streptavidin T1, Invitrogen, Life Technologies, Grand Island, NY, USA) was washed using BWB, a bar magnet, and vortexer. The beads were then added to the ligation reaction product. Following a short incubation, the DNA-bead construct was added to the flow-chamber. These chambers were then rinsed with SB and observed on the microscope. A model of the DNA tether sample is shown in Figure 23.

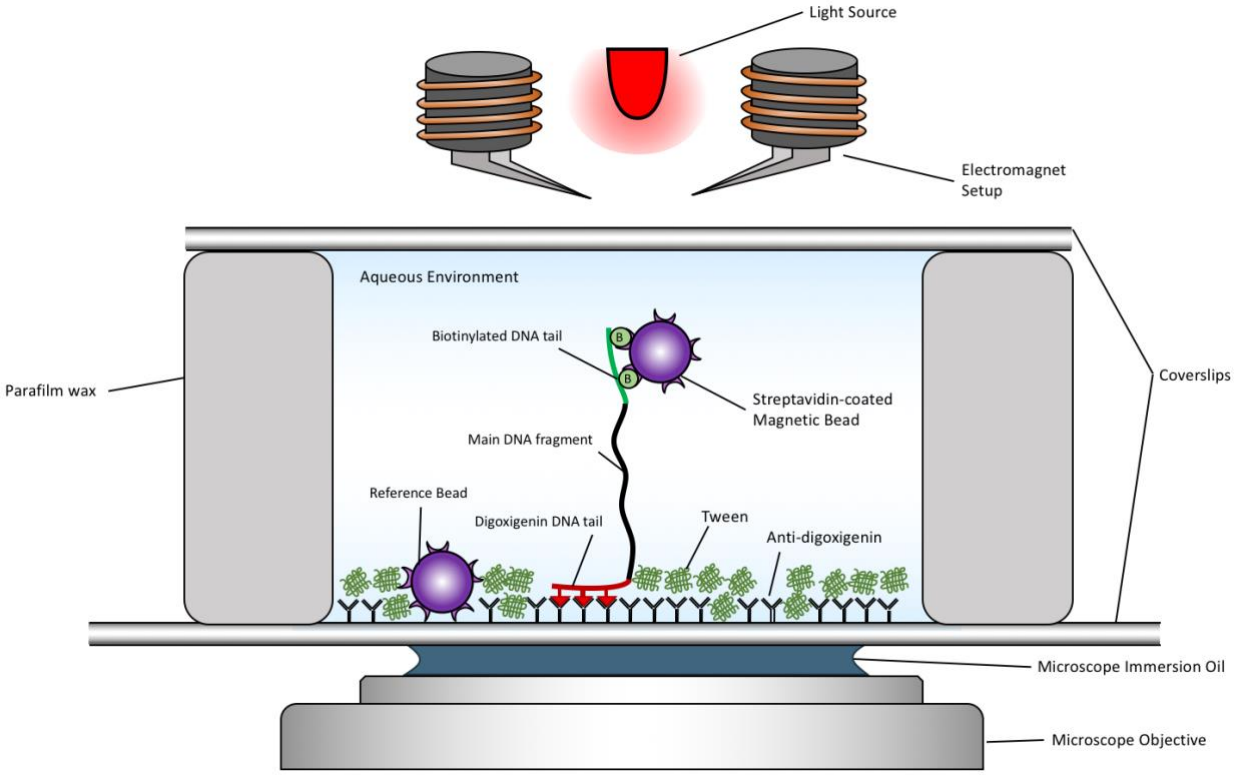

Figure 23: Experimental System Overview -To characterize the force regimes of interest, the interactions of the electromagnetic tweezers with a dsDNA tether sample were measured via light microscopy. The light source and magnetic tweezer setup are mounted above the flow-chamber housing the DNA tethers being studied. In the aqueous environment, the DNA construct is affixed to the anti-digoxigenin coated glass surface via its digoxigenin labelled tail. The free-end is attached to a streptavidin-coated magnetic bead. Nearby, a reference bead is nonspecifically bound to the glass surface. The surface is also coated in Tween to prevent further nonspecific binding. These DNA tethers are observed through a microscope objective mounted below.

C. Particle Tracking and Microscopy

The effective tether length ℓ is a crucial quantity in single-molecule DNA experiments. Magnetic tweezer microscopes are light-based systems that take advantage of diffraction to track beads and determine ℓ. The wavelength of the red LED light source (0.635 μm) and the diameter of the beads in the sample (1 μm) are of similar scale, generating a circular diffraction pattern of the beads at some specified objective focal plane (OFP). The raw images have units of pixels and must be converted to physical lengths using a calibration slide. If we establish the origin of a cartesian coordinate system at a DNA tether's point of attachment as depicted in Figure 24, the average effective tether length for some time interval is

$$\langle \ell \rangle = \frac{1}{n}\sum_{i=1}^{n}\left(\delta x_i^2 + \delta y_i^2 + \delta z_i^2\right)^{1/2}. \tag{17}$$

n is the number of images taken in the time interval while the indexed coordinates (δx_i, δy_i, and δz_i) are the bead's displacement coordinates in each image with respect to the origin.

Image analysis is required to properly calcuate δx, δy, and δz. Computer software establishes the center of the diffraction pattern by radial symmetry detection and assigns it an x' and y' coordinate. After executing constrained Brownian motion for some time interval, δx and δy at some time can be expressed as

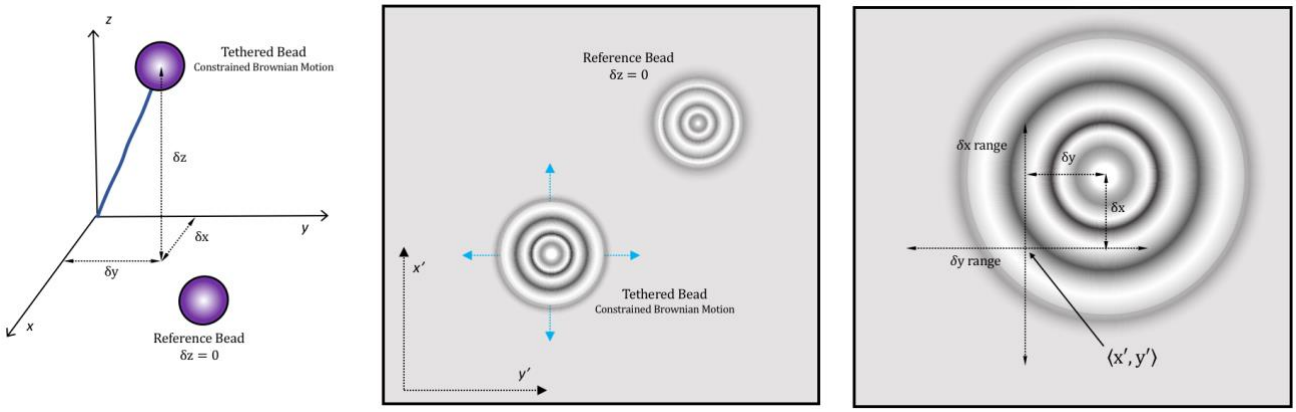

Figure 24: Particle Tracking Overview- **Left-** The DNA/bead system is mathematically described by the diagram shown. The origin of a cartesian coordinate system is at the anchoring point of the DNA, while the coordinates δx, δy, and δz represent the bead's position. In each experimental field of view, a reference bead must be present to calculate δz. **Middle-** A model field of view with a tethered bead and reference bead. The two beads not only possess different diffraction patterns, but different characteristic motions as well. Tethered beads exhibit constrained Brownian motion in the x' and y' directions while reference beads appear stationary. **Right-** For a bead executing constrained Brownian motion, the average x' and y' positions are regarded as the anchor point/cartesian coordinate origin. The deviations from $\langle x', y' \rangle$ are δx and δy.

$$\delta x = x' - \langle x' \rangle \quad (18)$$

$$\delta y = y' - \langle y' \rangle. \quad (19)$$

The δz for each image is calculated by comparing the diffraction patterns of the DNA tether and a reference bead stuck to the glass, for which we assume z = 0. For each frame in a video sequence, the computer algorithm determines the best match from a look up table generated by altering the OFP while recording diffraction patterns to determine the momentary position of the bead along the optical axis.[9,24] By extracting the bead's coordinates relative to its point of attachment, we can calculate the average effective tether length by equation (17). The effective tether length is then used to calculate the tension in the tether.

A microscope was specifically built to integrate the electromagnetic tweezer. A picture of this setup can be found in Figure 25. This setup was built around an Oriel Corporation optical post (Stratford, CT). A 635 nm LED light emitter (Mouser Electronics) fixed into a custom-made collimator begins the optical train. The light travels down through the microscope axis and illuminates the sample placed on the stage. The piezoelectric objective mount (Pifoc/Physics Instruments, Germany) allows the nanometer positioning of the 60X objective (Leica, Germany) along the optical axis. After travelling through the objective, light from the sample is focused by a relay lens onto an acA2000-165um- Basler

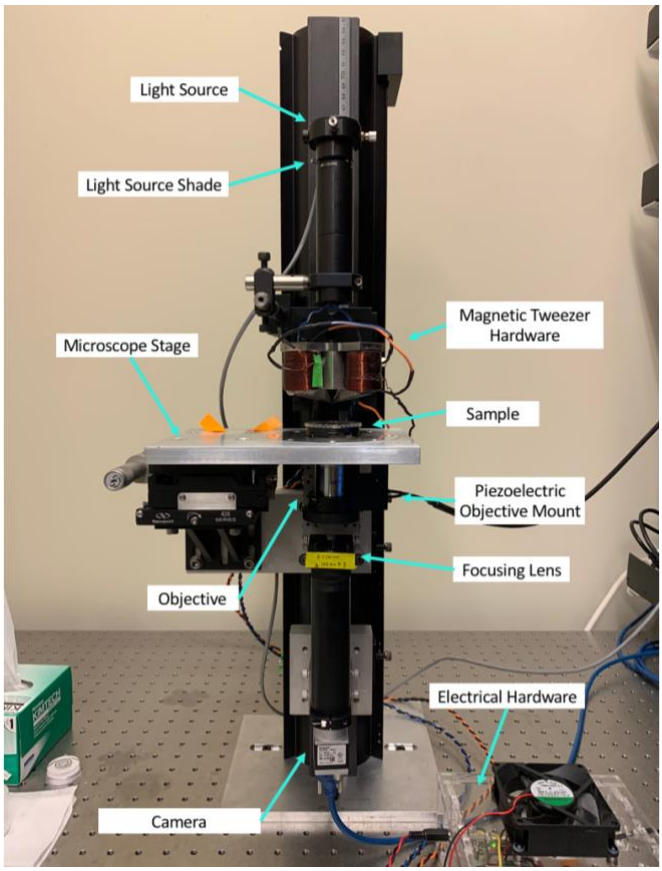

Figure 25: Electromagnetic Tweezer Microscope - The optical train begins with the light source and ends with the camera. This setup was built by Dr. Joshua Mendez during his tenure as a postdoc in the Finzi lab.

ace camera (Balser, Exton, PA). Finally, the camera passes live video information to the computer and custom Matlab (MathWorks, Waltham, MA) microscopy software.

D. Force Calculations

The attractive force achieved by magnetic tweezers can be calculated from the particle tracking parameters δx and δy. To derive an expression for force, we can analyze the system pictured in Figure 26. We begin by describing the total potential energy of the DNA tether (U_{sys}) as

$$U_{sys} = U_B + U_{DNA}\,, \tag{20}$$

where U_B (J) is the potential energy due to the magnetic field and U_{DNA} (J) is the potential energy from the DNA itself. U_{DNA} originates from the DNA's efforts to adopt an energetically favorable conformation dependent on $\boldsymbol{\ell}$, which we can call $A(\boldsymbol{\ell})$. This gives us

$$U_{DNA} = A(\boldsymbol{\ell})\,. \tag{21}$$

The magnetic force is essentially conservative on the sample because its direction and magnitude vary negligibly in the constrained range of motion. Due to this we can derive U_B as a function of δz the following way:

$$F = -\frac{dU_B}{dz}$$

$$\int_0^{U_B} dU_B = -F\int_0^{\delta z} dz$$

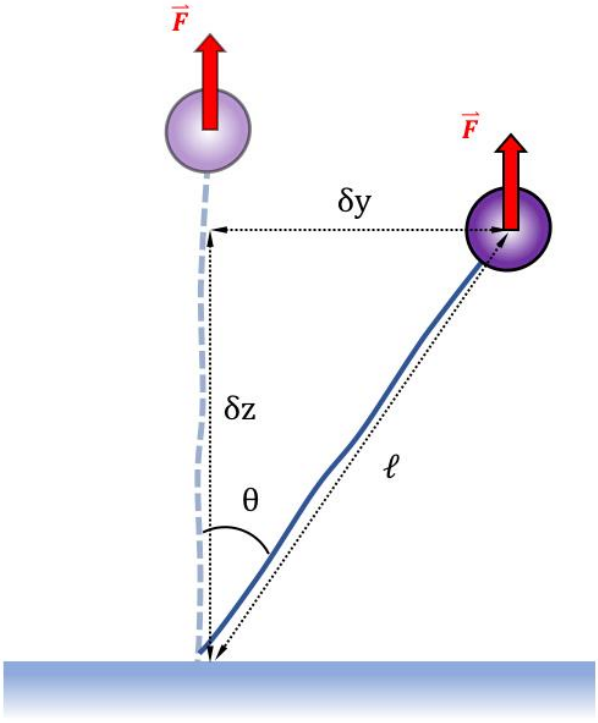

Figure 26: Attractive Force Model System - A DNA tether in the MT setup resembles an inverted pendulum. The dotted line shows the equilibrium position of the DNA tether when executing constrained Brownian motion along the y-axis. The δy and δz positions are shown for the DNA tether at some arbitrary non-equilibrium position. Attractive force is denoted by the red arrow pointing in the +z direction.

$$\mathrm{U_B}(\delta \mathrm{z}) = -F\ \delta \mathrm{z} \tag{22}$$

This is possible because we set the magnetic potential to 0 at the surface where z is 0. By combining equations (21) and (22) into equation (20), we find the potential of the system to be

$$\mathrm{U_{sys}} = \mathrm{A}(\boldsymbol{\ell}) - F\ \delta \mathrm{z}\,. \tag{23}$$

When the bead is in its equilibrium position, δx and δy are 0 while δz is ℓ. This equilibrium position ($\mathbf{r_o}$) can be mathematically described as

$$\mathbf{r_o} = \delta \mathrm{x}_o \hat{\boldsymbol{x}} + \delta \mathrm{y}_o \hat{\boldsymbol{y}} + \delta \mathrm{z}_o \hat{\boldsymbol{z}} = \ell\ \hat{\boldsymbol{z}}\,. \tag{24}$$

In this equilibrium position the first partial derivative of potential energy in x, y, and z are 0, or

$$\frac{\partial \mathrm{U_{sys}}(\delta \mathrm{x}_o)}{\partial \mathrm{x}} = \frac{\partial \mathrm{U_{sys}}(\delta \mathrm{y}_o)}{\partial \mathrm{y}} = \frac{\partial \mathrm{U_{sys}}(\delta \mathrm{z}_o)}{\partial \mathrm{z}} = 0\,. \tag{25}$$

We can use a Taylor expansion to describe the system's potential in the y direction as a function of δy, giving us

$$\mathrm{U_{sys}}(\delta \mathrm{y}) = \mathrm{U_{sys}}(\delta \mathrm{y_o}) + \frac{\partial \mathrm{U_{sys}}(\delta \mathrm{y_o})}{\partial \mathrm{y}}(\delta \mathrm{y} - \delta \mathrm{y_o}) + \frac{1}{2}\frac{\partial^2 \mathrm{U_{sys}}(\delta \mathrm{y_o})}{\partial \mathrm{y}^2}(\delta \mathrm{y} - \delta \mathrm{y_o})^2 \tag{26}$$

The only quantity needed now is the second partial derivative of the system's potential energy at the equilibrium position. This can be found by making a simple Pythagorean substitution for δz in equation (23) and taking the second partial derivative with respect to y.

$$\mathrm{U_{sys}}(\delta \mathrm{y}) = \mathrm{A}(\boldsymbol{\ell}) - F\ (\boldsymbol{\ell}^2 - \delta \mathrm{y}^2)^{\frac{1}{2}}$$

$$\frac{\partial^2 \mathrm{U_{sys}}(\delta \mathrm{y})}{\partial \mathrm{y}^2} = \mathrm{F}\ \delta \mathrm{y}^2 (\ell^2 - \delta \mathrm{y}^2)^{-\frac{3}{2}} + \mathrm{F}(\ell^2 - \delta \mathrm{y}^2)^{-\frac{1}{2}}$$

$$\frac{\partial^2 \mathrm{U_{sys}}(\delta \mathrm{y} = 0)}{\partial \mathrm{y}^2} = \frac{\mathrm{F}}{\ell} \tag{27}$$

Using equations (25) and (27), equation (26) becomes

$$\mathrm{U_{sys}}(\delta \mathrm{y}) = \mathrm{U_{sys}}(\delta \mathrm{y_o}) + \frac{1}{2}\frac{\mathrm{F}}{\ell}\delta \mathrm{y}^2. \tag{28}$$

If we set the potential energy of the system at the equilibrium position to 0, the time-averaged potential energy of the system is expressed as

$$\langle \mathrm{U_{sys}} \rangle = \frac{1}{2}\frac{\mathrm{F}}{\langle \ell \rangle}\langle \delta \mathrm{y}^2 \rangle. \tag{29}$$

Additionally, according to the equipartition theorem, the average potential energy of the system for each degree of freedom is

$$\langle \mathrm{U_{sys}} \rangle = \frac{1}{2}\mathrm{k_B T}\,. \tag{30}$$

Maxwell Boltzmann's constant (1.38E-23 J/K) is k_B and T is the temperature (K). By combining equations (29) and (30) and rearranging the variables, the attractive force over some time period is

$$F = \frac{k_B T}{\langle \delta y^2 \rangle} \langle \ell \rangle = \frac{k_B T}{\langle \delta x^2 \rangle} \langle \ell \rangle . \quad (31)$$

The $\langle \delta x^2 \rangle$ version can be symmetrically derived due to the orthogonality between the x and y axes. Equation (31) shows the force can be calculated from $\langle \ell \rangle$ and the variance of position along the x or y, direction, both of which are quantities available through the particle tracking software. The data analysis software used in our experiments is available in Appendix B.

E. Testing the Electromagnet

Each sample was prepared identically for electromagnet testing. For each test, the electromagnet pole pieces were positioned at a constant height above the top coverslip and the power supply was set to 12 V. After the flow-chamber sample was loaded onto the microscope stage, the objective was raised to allow the objective oil to interface with the bottom coverslip. A custom MATLAB program was used to access the live camera feed. Once a field of view was obtained that included both beads executing constrained Brownian motion and beads stuck to the glass surface, particle tracking was initiated. After selecting the particles to be tracked, a calibration profile was taken from each bead to correlate each diffraction pattern shape with δz. Now, the individual DNA tethers in the field of view could be manipulated using the electromagnet. To test the attractive force and torque regimes of the electromagnet, several different tests were performed.

Force Extension curves. To test the attractive force, a force extension test was used. In this test, the direction of the magnetic field generated by the eMTs was held constant while its magnitude was manipulated. The pole pieces were positioned approximately 1.5 mm above the top coverslip. Beginning with eMT strength at 0%, tethered bead motion was tracked for 10 seconds. Then the magnet strength was then increased by 10% every 10 seconds to 100%. After a time interval at 100%, the strength was decreased by 10% every 10 seconds to 0%. Particle tracking recorded bead position for each interval. The ability of the electromagnet to successfully generate attractive force was tested in two ways. First, observing a correlation between electromagnet strength with effective tether length (by equation (17)) during intervals of stretching and relaxation of the DNA double helix. Second, by showing correlation between electromagnet strength and generated force (by equation (31)). The software used can be found in Appendix B.

Extension vs. Turns curves. To test torque, an extension versus turn test was used. In this test, the eMT magnetic field direction was manipulated while magnitude was held constant at 80%. The pole

pieces were positioned approximately 2.5 mm above the top coverslip. The magnetic field was first spun to -20 turns. Then, motion tracking was initiated and the turns of the field were incrementally increased to +20. Step size was set to 0.2, step period to 3 seconds, and the camera's capture limit at 40 Hz. This meant that at each incremental turn, about 120 images were captured. The average changes in recorded vertical bead height values (δz) versus turn number were then analyzed by a custom MATLAB program (software can be found in Appendix C).

Stepwise Curves. Additionally, the electromagnet's ability to adopt accurate and consistent forces was measured. Real paramagnetic materials, like the one utilized in the solenoid cores, are not perfectly paramagnetic. This leads to the magnetic domains "sticking" to the direction induced by the applied field, a phenomenon known as hysteresis. Hysteresis can manifest itself in the electromagnet's inability to decrease the field to previously set values. We measured the effects of hysteresis on generated force using this step-wise test. A baseline value was set (either 0% or 20%) for the first time interval of 15 seconds. After this, the magnet's strength was increased 20% above baseline for an interval followed by another interval at baseline. Then the magnet strength would be increased 40% above baseline for an interval and returned to baseline. This process was repeated incrementally until an interval was recorded after the 100% interval. This step-wise test was utilized to see if the attractive force would adopt consistent values.

IV. Results and Discussion

A. Force Extension Test

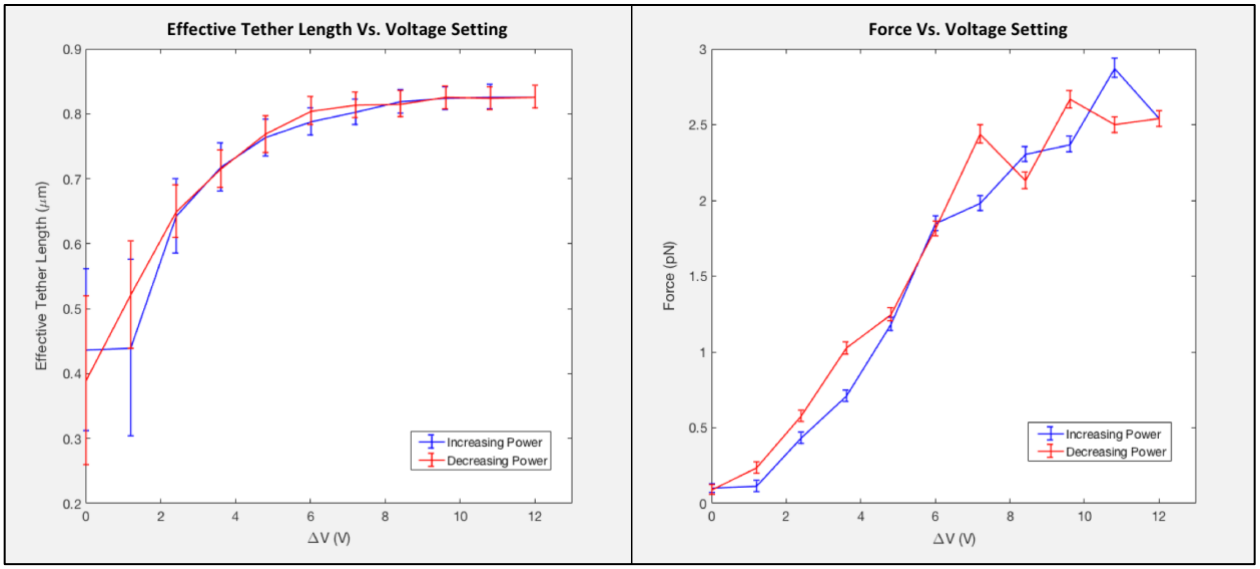

Figure 27: Force Extension Results- This graphic was generated in Matlab. The time intervals for the first half of the experiment, when power was incrementally increased, are shown in blue. The decreasing intervals are shown in red. The x axis for both graphs is the voltage difference setting for the active set of coils in volts. Both of these tests were performed on the same DNA tether. **Left-** Effective tether length versus voltage setting. This demonstrates that with increasing power setting the effective DNA tether length increases. The error bars are the standard deviations in tether length during each time interval. **Right-** Attractive force (piconewtons) versus voltage setting. The error bars are calculated as a function of standard deviation of tether length and y variance.

The force extension test shows that DNA is stretched by the attractive force generated by the eMTs. The graphs in Figure 27 are from the same DNA tether. In the left panel, the effective tether length increases with the increasing voltage across the active solenoid pair. No hysteresis was detected between DNA stretching and relaxation based on the similarity between the blue and red curves. At low voltage values, large deviations from the mean for tether length are observed, as expected. This is because at lower voltage settings, and thus lower forces, the DNA tether has less constraints on its stochastic motion. The force graph shows that the generated attractive force is directly related to the voltage setting from the overall curve shape. The maximum force achieved is approximately 2.5 pN. For most of the voltage range, the attractive forces achieved while increasing power are lower than the decreasing power. This could possibly indicate that hysteresis is occurring in the solenoid cores. Furthermore, the slope of the force vs. voltage setting curve decreases at approximately 8 V. This feature, after testing various values of current in response to voltage on the power supply, is most likely

influenced by a power limit unintentionally set by the power supply. This power limit may decrease the performance of the electromagnet after the limit is reached, leading to this plateau. Further testing of the power supply is needed to confirm this. Overall, these results indicate that the electromagnet is capable of manipulating effective tether length via attractive force.

B. Extension vs. Turns Test

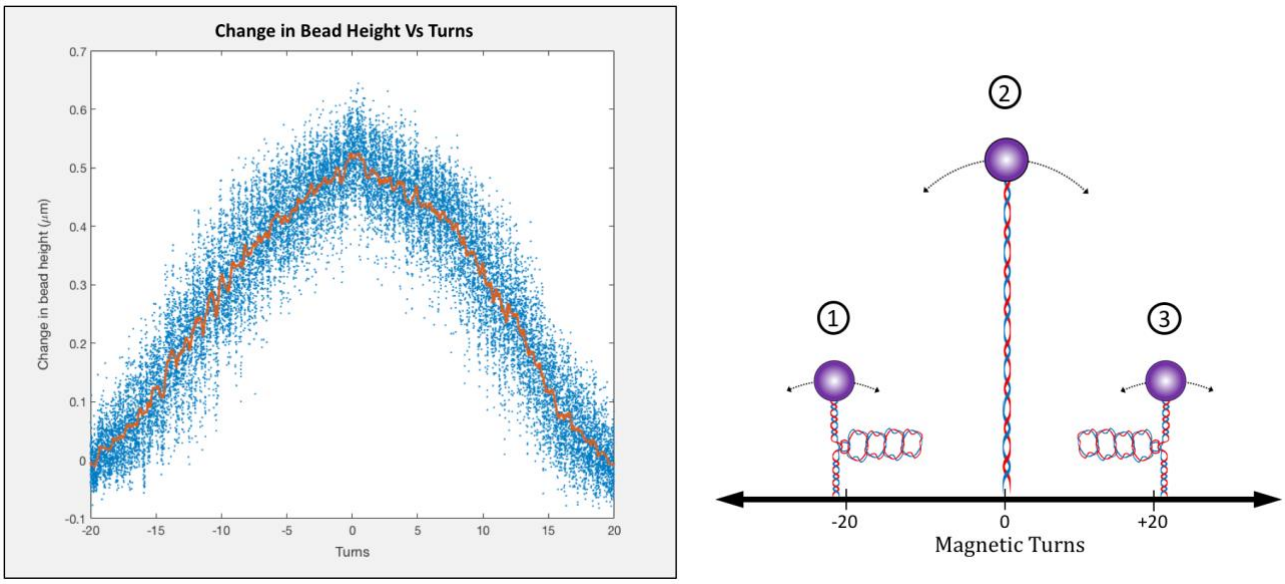

Figure 28: Extension Vs. Turns Results- **Left-** This graphic was generated in Matlab. The tether's z position at -20 turns was taken to be the initial z when calculating change in bead height (micrometers). The moving average (orange) of the changing z position (blue) increases and decreases symmetrically as turns are increased to +20. **Right-** A graphical representation of the DNA tether as it transitions from -20 to +20 turns with bead height (z position) as proxy for extension. Initially, the tether is very negatively supercoiled, inducing conformational change to a left-handed double-helix (Z-form) and the formation of loops, which decrease the average z position (1). As positive turning returns the DNA tether to its natural twist, the z position reaches a maximum value at 0 turns (2). As positive supercoiling continues, the DNA tether is induced to form plectonemes, and as a result the average z position decreases (3).

The extension versus turns test shows that the electromagnet is capable of supercoiling DNA. Under low tension, dsDNA that is twisted below the so called buckling transition will form plectonemes. As more turns are introduced into the molecule, more plectonemes are induced, shortening the DNA tether's vertical height. In Figure 28, the recorded δz values relative to the initial δz at -20 turns are shown by the blue scattered data points. A moving average of these δz values was taken, shown in orange. Due to the experiment start point at -20 turns, the bead height is at a local minimum. As we apply torque to the tethered bead towards 0 turns, the plectonemes are no longer induced and vertical height increases. As we move beyond the natural twist of the double-helix at 0 turns, plectoneme

formation is again induced, reducing the average height of the molecule. At 0 turns, a small spike in average bead height occurs. This graphical feature may suggest the bead is tethered by 2 separate dsDNA molecules. Regardless, the electromagnet's torque capability is confirmed because doubly-tethered beads exhibit similar looping behavior as single-tethered molecules.[15] At the salt concentration of stretching buffer (100 mM), the symmetric curve in Figure 28 suggests an attractive force of less than 1 pN.[9] The electromagnet's ability to introduce turns, via torque, into DNA tethers is confirmed by this curve.

C. Stepwise Tests

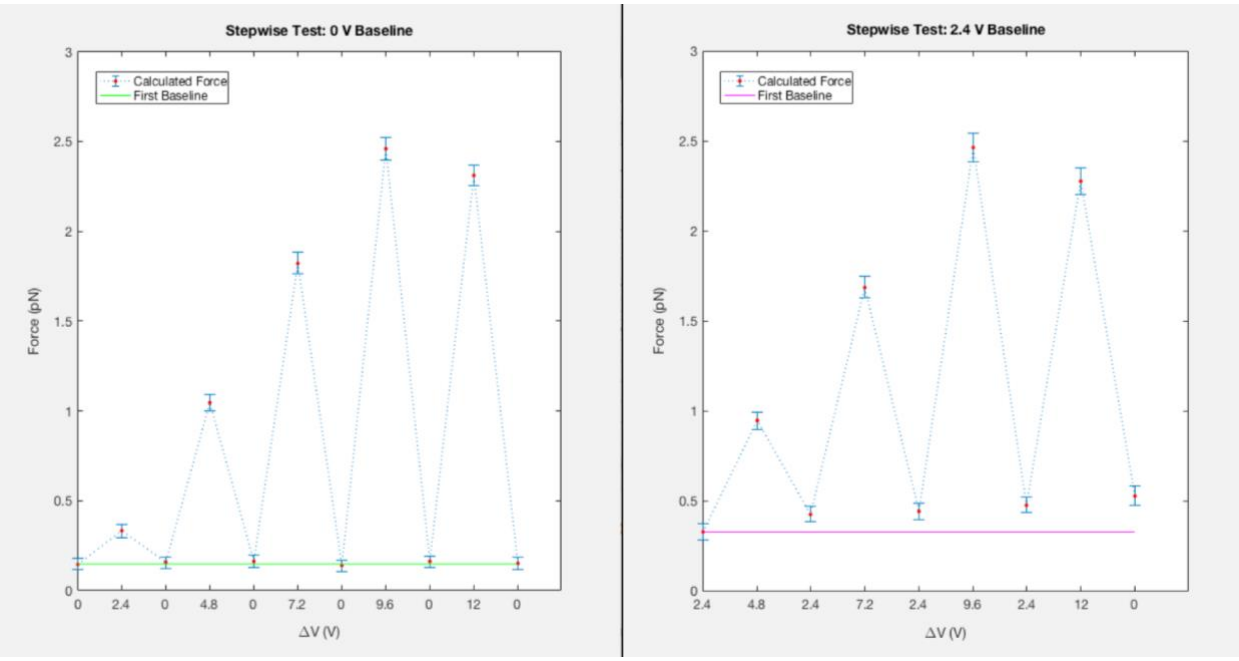

Figure 29: Stepwise Test Results- The x and y axes are voltage setting (volts) and force (piconewtons), respectively. The calculated force at each voltage setting interval is shown as a red dot with a function of y variance and length standard deviation for error bars. The first voltage setting was treated as the baseline force value. Both tests were performed on the same DNA tether. **Left-** A horizontal green line denotes the initial force for the baseline voltage setting. The electromagnet effectively achieves consistent forces when returning to a 0V baseline. **Right-**A horizontal purple line denotes the initial force for the baseline voltage setting. The electromagnet's generated attractive force does not return to 2.4 V baseline effectively.

This test (Figure 29) shows that the electromagnet is capable of switching force values accurately. For the 0 V baseline test, the manipulation of voltage settings directly changed the attractive force exerted. Furthermore, the electromagnet returned to the baseline force with great accuracy, demonstrated by the return to 0 V values within a standard deviation of the original baseline. In the 2.4 V baseline test, deviations from the baseline increased as the prior voltage value increased. The

difference in return-to-baseline ability between these two step-wise tests suggests that the solenoid cores are more affected by hysteresis when current runs through the coils. This means the electromagnet can 'turn off' the field more easily than it can limit its magnitude. While hysteresis is a concern for force accuracy, we anticipate that its affects will be limited by the field changing polarity while executing turns. When the software manipulates current to create turns, the field in each respective magnet flips frequently. This flipping can serve to degauss the residual magnetism leftover from experiments where the field direction is constant. In comparison with the force extension test, this data shows a similar plateau of achieved force at 2.5 pN.

D. Future Aims

Technical improvements. Further testing of the hysteresis effects on force consistency are required. One possible test could include a step-wise test with an added 'degaussing' spin cycle between intervals. A number of improvements are planned for the electromagnetic tweezers in the future. Adding a liquid cooling system to the magnetic tweezer frame would help mitigate long term damage to the electrical components caused by heat erosion. Additionally, the pole piece geometry can be tuned to improve net B field on the sample. Switching to a 4 channel system instead of the current 2 channel system is also a possible improvement. Because the existing circuit is 2 pairs of solenoid coils wired in series, the overall resistance in each respective pair limits the maximum current. If each coil was wired separately, the overall resistance would decrease for each current channel, allowing us to achieve higher currents, inducing higher B fields and higher forces. Furthermore, individual wiring would allow the user to tune the current through each individual coil. Ultimately the Finzi lab hopes to consolidate the electromagnetic tweezer into a smaller, portable system that can be integrated into a greater variety of microscopy systems.

Biological applications. The eMT microscope is ideal to study any biological interaction that is sensitive to vibrations, or requires an almost instantaneous change in the strength of the magnetic field. Applications are not limited to transcription, nor to DNA. Indeed, any nucleic acid transaction, or biomechanical process at the molecular scale, such as the activation of large muscle proteins by ligands, can be studied with this instrument.

V. Works Cited

1. Pukkila, P. J. Molecular Biology: The Central Dogma. *eLS* (2001). doi:doi:10.1038/npg.els.0000812
2. Finzi, L. & Olson, W. K. The emerging role of DNA supercoiling as a dynamic player in genomic structure and function. *Biophys. Rev.* **8**, 1–3 (2016).
3. Yan, Y., Leng, F., Finzi, L. & Dunlap, D. Protein-mediated looping of DNA under tension requires supercoiling. *Nucleic Acids Res.* **46**, 2370–2379 (2018).
4. Vörös, Z., Yan, Y., Kovari, D. T., Finzi, L. & Dunlap, D. Proteins mediating DNA loops effectively block transcription. *Protein Sci.* **26**, 1427–1438 (2017).
5. Yan, Y., Ding, Y., Leng, F., Dunlap, D. & Finzi, L. Protein-mediated loops in supercoiled DNA create large topological domains. *Nucleic Acids Res.* **46**, 4417–4424 (2018).
6. Matthews, K. S. DNA looping. *Microbiol. Rev.* **56**, 123 LP – 136 (1992).
7. Goodsell, D. S. lac Repressor. *RCSB Protein Data Bank* (2003). doi:10.2210/rcsb_pdb/mom_2003_3
8. Smith, S. B., Finzi, L. & Bustamante, C. Direct mechanical measurements of the elasticity of single DNA molecules by using magnetic beads. *Science (80-.).* **258**, 1122 LP – 1126 (1992).
9. Vilfan, I. D., Lipfert, J., Koster, D. A., Lemay, S. G. & Dekker, N. H. Magnetic Tweezers for Single-Molecule Experiments BT - Handbook of Single-Molecule Biophysics. in (eds. Hinterdorfer, P. & Oijen, A.) 371–395 (Springer US, 2009). doi:10.1007/978-0-387-76497-9_13
10. White, J. H. Self-Linking and the Gauss Integral in Higher Dimensions. *Am. J. Math.* **91**, 693–728 (1969).
11. Vilfan, I., Lipfert, J., Koster, D., Lemay, S. & Dekker, N. Magnetic Tweezers for Single-Molecule Experiments. in 371–395 (1970). doi:10.1007/978-0-387-76497-9_13
12. Finzi, L. & Dunlap, D. D. Single-molecule approaches to probe the structure, kinetics, and thermodynamics of nucleoprotein complexes that regulate transcription. *J. Biol. Chem.* **285**, 18973–18978 (2010).
13. Travers, A. & Muskhelishvili, G. DNA structure and function. *FEBS J.* **282**, 2279–2295 (2015).
14. Roca, J. The torsional state of DNA within the chromosome. *Chromosoma* **120**, 323–334 (2011).
15. Charvin, G., Bensimon, D. & Croquette, V. Single-molecule study of DNA unlinking by eukaryotic and prokaryotic type-II topoisomerases. *Proc. Natl. Acad. Sci.* **100**, 9820 LP – 9825 (2003).
16. Seol, Y., Strub, M.-P. & Neuman, K. C. Single molecule measurements of DNA helicase activity with magnetic tweezers and t-test based step-finding analysis. *Methods* **105**, 119–127 (2016).
17. Revyakin, A., Ebright, R. H. & Strick, T. R. Promoter unwinding and promoter clearance by RNA

polymerase: Detection by single-molecule DNA nanomanipulation. *Proc. Natl. Acad. Sci. U. S. A.* **101**, 4776 LP – 4780 (2004).

18. Griffiths, D. J. (Reed C. *Introduction to Electrodynamics*. (Pearson, 2013).
19. Naqib, A., Poggi, S. & Green, S. J. Deconstructing the Polymerase Chain Reaction II: an improved workflow and effects on artifact formation and primer degeneracy. *PeerJ* **7**, e7121–e7121 (2019).
20. Lee, P. Y., Costumbrado, J., Hsu, C.-Y. & Kim, Y. H. Agarose gel electrophoresis for the separation of DNA fragments. *J. Vis. Exp.* 3923 (2012). doi:10.3791/3923
21. Narayanan, J., Xiong, J.-Y. & Liu, X.-Y. Determination of agarose gel pore size: Absorbance measurements vis a vis other techniques. *J. Phys. Conf. Ser.* **28**, 83–86 (2006).
22. Belkebir, A. & Azeddoug, H. Metal ion dependence of DNA cleavage by SepMI and EhoI restriction endonucleases. *Microbiol. Res.* **168**, 99–105 (2013).
23. Pan, H., Xia, Y., Qin, M., Cao, Y. & Wang, W. A simple procedure to improve the surface passivation for single molecule fluorescence studies. *Phys. Biol.* **12**, 45006 (2015).
24. Kovari, D. T., Dunlap, D., Weeks, E. R. & Finzi, L. Model-free 3D localization with precision estimates for brightfield-imaged particles. *Opt. Express* **27**, 29875–29895 (2019).

VI. Appendix

A. pDD_IN2BbvCI Plasmid

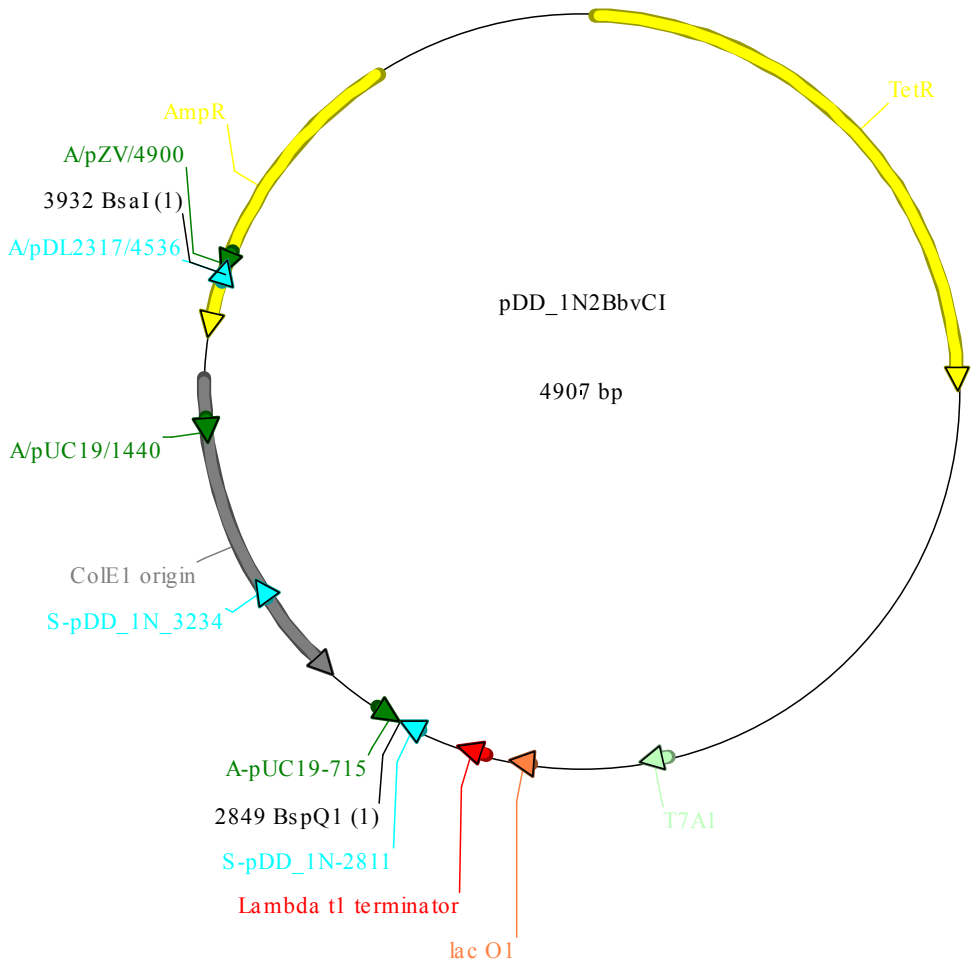

Sequence:

tatcacagttaaattgctaacgcagtcaggcaccgtgtatgaaatctaacaatgcgctcatcgtcatcctcggcaccgtcaccctggatgctgtaggca
taggcttggttatgccggtactgccgggcctcttgcgggatatcgtccattccgacagcatcgccagtcactatggcgtgctgctagcgctatatgcgttg
atgcaatttctatgcgcacccgttctcggagcactgtccgaccgctttggccgccgcccagtcctgctcgcttcgctacttggagccactatcgactacgc
gatcatggcgaccacacccgtcctgtggatcctctacgccggacgcatcgtggccggcatcaccggcgccacaggtgcggttgctggcgcctatatcg
ccgacatcaccgatggggaagatcgggctcgccacttcgggctcatgagcgcttgtttcggcgtgggtatggtggcaggccccgtggccgggggactg
ttgggcgccatctccttgcatgcaccattccttgcggcggcggtgctcaacggcctcaacctactactgggctgcttcctaatgcaggagtcgcataagg
gagagcgtcgaccgatgcccttgagagccttcaacccagtcagctccttccggtgggcgcggggcatgactatcgtcgccgcacttatgactgtcttctt
tatcatgcaactcgtaggacaggtgccggcagcgctctgggtcattttcggcgaggaccgctttcgctggagcgcgacgatgatcggcctgtcgcttgc
ggtattcggaatcttgcacgccctcgctcaagccttcgtcactggtcccgccaccaaacgtttcggcgagaagcaggccattatcgccggcatggcggc
cgacgcgctgggctacgtcttgctggcgttcgcgacgcgaggctggatggccttccccattatgattcttctcgcttccggcggcatcgggatgcccgcg
ttgcaggccatgctgtccaggcaggtagatgacgaccatcagggacagcttcaaggatcgctcgcggctcttaccagcctaacttcgatcattggaccg
ctgatcgtcacggcgatttatgccgcctcggcgagcacatggaacgggttggcatggattgtaggcgccgccctataccttgtctgcctccccgcgttgc
gtcgcggtgcatggagccgggccacctcgacctgaatggaagccggcggcacctcgctaacggattcaccactccaagaattggagccaatcaattct
tgcggagaactgtgaatgcgcaaaccaaccccttggcagaacatatccatcgcgtccgccatctccagcagccgcacgcggcgcatctcgggcagcgtt
gggtcctggccacgggtgcgcatgatcgtgctcctgtcgttgaggacccggctaggctggcggggttgccttactggttagcagaatgaatcaccgata

cgcgagcgaacgtgaagcgactgctgctgcaaaacgtctgcgacctgagcaacaacatgaatggtcttcggtttccgtgtttcgtaaagtctggaaac
gcggaagtcagcgccctgcaccattatgttccggatctgcatcgcaggatgctgctggctaccctgtggaacacctacatctgtattaacgaagcgctg
gcattgaccctgagtgatttttctctggtcccgccgcatccataccgccagttgtttaccctcacaacgttccagtaaccgggcatgttcatcatcagtaa
cccgtatcgtgagcatcctctctcgtttcatcggtatcattacccccatgaacagaaatcccccttacacggaggcatcagtgaccaaacaggaaaaaa
ccgcccttaacatggcccgctttatcagaagccagacattaacgcttctggagaaactcaacgagctggacgcggatgaacaggcagacatctgtga
atcgcttcacgaccacgctgatgagctttaccgcagctgcctcgcgcgtttcggtgatgacggtgaaaacctctgacacatgcagctcccggagacggt
cacagcttgtctgtaagcggatgccgggagcagacaagcccgtcagggcgcgtcagcgggtgttggcAggtgtcggggcgcagccatgacccagtc
accccatggtgcagtatgaaggcggcggagccgacaccacggccaccgatattatttgcccgatgtacgcgcgcgtggatgaaCaccagcccttccc
ggctttatcaaaaagagtattgacttaaagtctaacctataggatacttacagcgatggagaggtgtagtggtaaccagaagataagatggctttcgct
acctggagagacgcgcccgctgatcctttgcgaatacgcccacgcgatgggtaacagtcttggcggtttcgctaaatactggcaggcgtttcgtcagta
tccccgtttacagggcggcttcgtctgggactgggtggatcagtcgctgattaaatatgatgaaaacggcaacccgtggtacctcagcctgcggaaatt
gtgagcggataacaattaacctccctcagcggccgcaagaaaactatcccgaccgccttactgccgcctgttttgaccgctgggatctgctgtaacaga
gcattagcgcaaggtgatttttgtcttcttgcgctaatttttttccattgtctagagtagcgatagcggagtgtatactggcttaactatgcggcatcagagc
agattgtactgagagtgcaccatatgcggtgtgaaataccgcacagatgcgtaaggagaaaataccgcatcaggcgctcttccgcttcctcgctcact
gactcgctgcgctcggtcgttcggctgcggcgagcggtatcagctcactcaaaggcggtaatacggttatccacagaatcaggggataacgcaggaa
agaacatgtgagcaaaaggccagcaaaaggccaggaaccgtaaaaaggccgcgttgctggcgtttttccataggctccgccccccctgacgagcatca
caaaaatcgacgctcaagtcagaggtggcgaaacccgacaggactataaagataccaggcgtttcccccctggaagctccctcgtgcgctctcctgttc
cgaccctgccgcttaccggatacctgtccgcctttctcccttcgggaagcgtggcgctttctcatagctcacgctgtaggtatctcagttcggtgtaggtc
gttcgctccaagctgggctgtgtgcacgaaccccccgttcagcccgaccgctgcgccttatccggtaactatcgtcttgagtccaacccggtaagacac
gacttatcgccactggcagcagccactggtaacaggattagcagagcgaggtatgtaggcggtgctacagagttcttgaagtggtggcctaactacgg
ctacactagaaggacagtatttggtatctgcgctctgctgaagccagttaccttcggaaaaagagttggtagctcttgatccggcaaacaaaccaccgc
tggtagcggtggttttttgtttgcaagcagcagattacgcgcagaaaaaaaggatctcaagaagatcctttgatcttttctacggggtctgacgctcag
tggaacgaaaactcacgttaagggattttggtcatgagattatcaaaaaggatcttcacctagatccttttaaattaaaaatgaagttttaaatcaatct
aaagtatatatgagtaaacttggtctgacagttaccaatgcttaatcagtgaggcacctatctcagcgatctgtctatttcgttcatccatagttgcctga
ctccccgtcgtgtagataactacgatacgggagggcttaccatctggccccagtgctgcaatgataccgcgagacccacgctcaccggctccagattta
tcagcaataaaccagccagccggaagggccgagcgcagaagtggtcctgcaactttatccgcctccatccagtctattaattgttgccgggaagctag
agtaagtagttcgccagttaatagtttgcgcaacgttgttgccattgctgcaggcatcgtggtgtcacgctcgtcgtttggtatggcttcattcagctccg
gttcccaacgatcaaggcgagttacatgatcccccatgttgtgcaaaaaagcggttagctccttcggtcctccgatcgttgtcagaagtaagttggccg
cagtgttatcactcatggttatggcagcactgcataattctcttactgtcatgccatccgtaagatgcttttctgtgactggtgagtactcaaccaagtcat
tctgagaatagtgtatgcggcgaccgagttgctcttgcccggcgtcaacacgggataataccgcgccacatagcagaactttaaaagtgctcatcattg
gaaaacgttcttcggggcgaaaactctcaaggatcttaccgctgttgagatccagttcgatgtaacccactcgtgcacccaactgatcttcagcatcttt
tactttcaccagcgtttctgggtgagcaaaaacaggaaggcaaaatgccgcaaaaaagggaataagggcgacacggaaatgttgaatactcatact
cttccttttcaatattattgaagcatttatcagggttattgtctcatgagcggatacatatttgaatgtatttagaaaaataaacaaataggggttccgc
gcacatttccccgaaaagtgccacctgacgtctaagaaaccattattatcatgacattaacctataaaaataggcgtatcacgaggccctttcgtcttca
agaattctcatgtttgacagcttatcatcgataagctttaatgcggtagtt

B. Force Extension Software

11/24/20 11:52 AM /Volume.../plot_LiveXYZForceExtensions.m 1 of 4

```
% [header,LiveData] = LoadLiveData();
%%
close all;

PWRsupplyVoltage = 12;
timeCushion = 2;
%time values near electromagnet setting transitions that we should
%eliminate due to possible timing issues

OilOffset = 0.8;

ApplyZOffset = false; %shift the dz positions so that zero magnet gives dz=0
ApplyOilOffset = true; %account for change in index of refraction, length are smaller

T = ([LiveData.Date]-LiveData(1).Date)*24*3600;
%change time values of each data point to elapsed time from onset of
%experiment

dZ = [LiveData.dZ]; %dZ from data is (Z_ABS - Z_REL)
X = [LiveData.X]; %raw pixel X locations of beads
Y = [LiveData.Y]; %raw pixel Y locations of beads

kBT=1.380648813e-23*(273.15+header.Temperature)*10^6;

X2 = X;
Y2 = Y;

[numBeads, flubs] = size(X2);


%% RECORD Time Steps and Coresponding Magnet Strengths here
Tstep = [0, 10, 20, 30, 40, 50, 60, 70, 80, 90, 100 , 110, 120, 130, 140, 150, 160, 170,↙
180, 190, 200, 210]; %use for 10s intervals
% Tstep = [0, 60, 120, 180, 240, 300, 360, 420, 480, 540, 600 , 660, 720, 780, 840, 900,↙
960, 1020, 1080, 1140, 1200, 1260]; %use for 60s intervals
Mag = [ 0, 25.5, 51, 76.5, 102, 127.5, 153, 178.5, 204, 229.5, 255, 229.5, 204, 178.5,↙
153, 127.5, 102, 76.5, 51, 25.5, 0];

[maxMagVal, midpt] = max(Mag);
%%
dZ2 = dZ;
Avg_dZ = NaN(numBeads, length(Tstep));
%creates array of NaN values the same size as Tstep array.


%% Avg position of tethers
goodT = T>(Tstep(1)+ timeCushion) & T<(Tstep(2)- timeCushion);
goodT2 = repmat(goodT, numBeads, 1);
%establish first range of values 0-10 seconds that we want to calculate our
%values
x_avg = NaN(numBeads,1);
y_avg = NaN(numBeads,1);

for n=1:numBeads
    x_avg(n) = nanmean(X2(n,:));
    y_avg(n) = nanmean(Y2(n,:));
    %Find first interval (0-10s)mean value of X/Y-values ignoring NaN values
    X2(n,:) = (X2(n,:)-x_avg(n))*header.PxScale;
```

```
    Y2(n,:) = (Y2(n,:)-y_avg(n))*header.PxScale;
    %Rewrite X2 values from pixels (coordinates on screen) to actual deviations
    %from an average position. It then converts this 'pixel' distance to a
    %physical distance (um)
end

%% Calculate
AvgF = NaN(numBeads,numel(Tstep)-1);
FErr = NaN(numBeads,numel(Tstep)-1);
Sig = NaN(numBeads,numel(Tstep)-1);
AvgLs = NaN(numBeads,numel(Tstep)-1);
eccentricity = NaN(numBeads, numel(Tstep)-1);
StdLs = NaN(numBeads, numel(Tstep)-1);

%create arrays of NaN values that will be populated later. The
%size is the size we will graph. Size is Tstep - 1 because Tstep has
%one extra value, but is actually representing the intervals between those
%time values.

for m=1:numBeads
    for n=2:numel(Tstep)
        goodT = T>(Tstep(n-1)+timeCushion) & T<(Tstep(n)-timeCushion);
        Avg_dZ(m,n) = nanmean(dZ2(m, goodT)); %mean of z positions during interval
        Sig(m,n) = nanstd(dZ2(m, goodT)); %std deviation of z position
        var_x = nanvar(X2(m, goodT)); %variance of x during interval
        var_y = nanvar(Y2(m, goodT)); %variance of y during interval

        if ApplyZOffset %see notes, not really sure why you would want this
            zz = dZ2(m, goodT) - Avg_dZ(m,2);
        else
            zz = dZ2(m, goodT);
        end

        L = sqrt( zz.^2 + X2(m, goodT).^2 + Y2(m, goodT).^2); %calculate length of tether↙
during interval
        avgL = nanmean(L); %take average of those individual tether lengths during↙
interval

        if ApplyOilOffset %apply oil offset or not
            avgL = OilOffset * avgL;
        else
            avgL = avgL;
        end

        StdL = nanstd(L); % find standard deviation of length values over interval

        StdLs(m,n-1) = StdL;
        AvgF(m,n-1) = kBT*avgL/var_y; % calculate average force for interval
        FErr(m,n-1) = kBT*StdL/var_y; % calculate error bar values for interval
        AvgLs(m,n-1) = avgL; % add average length values to array
        eccentricity(m,n-1) = var_y/var_x; %calculate eccentricity of motion based on x/y↙
variance
    end
end

%
%
% %% Plot
```

```
% % figure(1);clf;
% % errorbar(Mag,Avg_dZ,Sig)
% % ylabel('dZ [µm]');
% % xlabel('ElectroMagnet Strength (A.U.)');
% %
% % other way
% % figure(2);clf
% % errorbar(Avg_dZ,Mag,Sig,'horizontal');
% % set(gca,'YScale','Log');
% % xlabel('dZ [µm]');
% % ylabel('ElectroMagnet Strength (A.U.)');
%
%% Force Plots

plotAvgF = AvgF/1e-12;
plotFerr = FErr/1e-12;
beadVals = 1:1:numBeads;
MaxLs = max(AvgLs, [], 2);
voltageVals = linspace(0,PWRsupplyVoltage, ceil(length(Mag)/2));
plotVoltages = horzcat( voltageVals , flip(voltageVals(1:end-1)));


for i=1:numBeads
    %plot voltage setting vs. force
    figure();
    ascendingVals = plotAvgF(i,1:midpt);
    descendingVals = plotAvgF(i,midpt:end);
    errorbar(plotVoltages(1:midpt), ascendingVals ,plotFerr(i,1:midpt), 'b', 'Linewidth',↙
1.5)
    hold on
    errorbar(plotVoltages(midpt:end), descendingVals ,plotFerr(i,midpt:end), 'r',↙
'Linewidth', 1.5)
    legend({'Increasing Power','Decreasing Power'}, 'Location', 'southeast')
    set(gca,'FontSize',15)
    xlim( [0 13] )
    hold off
    title(['Voltage Setting Vs. Force ' num2str(i) '  (Max Length = ' num2str(MaxLs(i)) '↙
\mum)' ]);
    ylabel('Force (pN)');
    xlabel('\DeltaV (V)');

    %plot voltage setting vs. tether extension
    figure();
    ascendingVals = AvgLs(i,1:midpt);
    descendingVals = AvgLs(i,midpt:end);
    errorbar(plotVoltages(1:midpt), ascendingVals ,StdLs(i,1:midpt), 'b', 'Linewidth',↙
1.5)
    hold on
    errorbar(plotVoltages(midpt:end), descendingVals ,StdLs(i,midpt:end), 'r',↙
'Linewidth', 1.5)
    legend({'Increasing Power','Decreasing Power'}, 'Location', 'southeast')
    set(gca,'FontSize',15)
    xlim( [0 13] )
    hold off
    title(['Voltage Setting Vs. Effective Tether Length ' num2str(i) '  (Max Length = '↙
num2str(MaxLs(i)) ' \mum)' ]);
    ylabel('Effective Tether Length (\mum)');
    xlabel('\DeltaV (V)');
```



```
end
```

C. Extension vs. Turns Software

11/24/20 11:54 AM /Volumes/JOEPI.../plot_LiveXYZHatCurve.m 1 of 3

```
% [header,LiveData] = LoadLiveData();
close all;


StepSize = 0.2;
StepPeriod = 3;
Turns = -20:StepSize:20;
TurnsGraph = -20:5:20;
ExpLength = length(Turns)*StepPeriod;
%Experiment parameters

ApplyOilOffset = true; %account for change in index of refraction, length are smaller
OilOffset = 0.8;


% Use this code to format live data for plotting

T = ([LiveData.Date]' - LiveData(1).Date)*24*3600; %time in seconds

dZ = [LiveData.dZ]';


 %concatenate and rotate dZ data
%   dZ = ...
%       [dZ_trk1(Time0), dZ_trk2(Time0),...
%        dZ_trk1(Time1), dZ_trk2(Time1),...
%        ...
%        dZ_trk1(TimeEnd), dZ_trk2(TimeEnd),...


%% Plot Data

figure();
%    replicate T so that it is same size as dZ
plot(repmat(T,1,size(dZ,2)), dZ,'-');
xlabel('Time (sec)');
ylabel('Approx. Tether Length (µm)');
title('Zrel: Particle height relative to refrence LUT');
%% Look at changes in Z_abs (doesn't use relative measurement)

Zabs = [LiveData.Z_ABS]';

% assuming track 1 is reference calculate drift
Z_drift = Zabs(:,1);
%Z_drift = Z_drift - Z_drift(1);

%filter the drift to eliminate noise
WINDOW = 60;
Z_drift_filt = movmean(Z_drift,WINDOW,1,'omitnan'); %moving average

%shift values to start at 0;
Z_drift = Z_drift - Z_drift_filt(1);
Z_drift_filt = Z_drift_filt - Z_drift_filt(1);


%alternative use last of unfiltered data, comment above if using this code
%Z_drift_filt(end+1:end+floor(WINDOW/2)-1) = X_drift(end-floor(WINDOW/2):end);
```

```
%plot drift
figure();
plot(T,Z_drift,'-');
hold on;
title('Drift based on refernce bead')
plot(T,Z_drift_filt,'-');
xlabel('time (sec)');
ylabel('z drift (µm)');

%% Correct measurement Data for drift
Z_exp = Zabs(:,2:end);

figure();
plot(repmat(T,1,size(Z_exp,2)),Z_exp);
title('Raw Zabs Data');
xlabel('time (sec)');
ylabel('Zabs: Height Relative to Calibration LUT (µm)');


Z_exp = bsxfun(@minus,Z_exp,nanmean(Z_exp(1:WINDOW,:),1)); %shift data to be zero for an↙
average of the first WINDOW points, you need to use matrix expansion here which is why we↙
have bsxfun


figure();
plot(repmat(T,1,size(Z_exp,2)),Z_exp);
title('Mean-shifted Zabs data');
xlabel('Time (sec)');
ylabel('Zabs-<Zabs>_{1:wind} (µm)');

Z_exp = bsxfun(@minus,Z_exp,Z_drift_filt); %subtract the drift from each column

%remember, Z position is in terms of objective position so if particle gets
%further away from objective (i.e. moves further away from glass) the Z_abs
%will decrease.
%Therefore we need to take the negative to get the relative tether change
Z_exp = -Z_exp;

if ApplyOilOffset %apply oil offset or not
    Z_exp = OilOffset * Z_exp;
else
    Z_exp = Z_exp;
end




%% Seperately Plot Drift corrected data
for i=1:size(Z_exp,2)
    figure();
    plot(T,Z_exp(:,i),...
        'LineStyle','none',...
        'Marker','.',...
        'MarkerSize',3);
    titlename=strcat('Drift-corrected change in particle ',num2str(i),' height');
    title(titlename)
    xlabel('Turns');
    ylabel('Change in bead height (\mum)');
```

```
    xlim( [0 ExpLength] )
    set(gca,'FontSize',15)
    xticks( linspace(0,ExpLength,length(TurnsGraph)) )
    xticklabels(num2cell(TurnsGraph));
    %add filtered data
    WIND_exp = 200;
    Z_exp_filt = movmean(Z_exp,WIND_exp,1,'omitnan');%%filter(ones(WIND_exp,1)/WIND_exp,↙
1,Z_exp); %moving average

    %shift time
    %Z_exp_filt = Z_exp_filt(floor(WIND_exp/2):end,:);
    %Z_exp_filt(end+1:end+floor(WIND_exp/2)-1,:) = NaN;

    hold on
    plot(T,Z_exp_filt(:,i),...
        'LineStyle','-',...
        'LineWidth', 3);
end
```